

1 **Storage, evolution, and mixing in basaltic eruptions from around the Okataina Volcanic**  
2 **Centre, Taupō Volcanic Zone, Aotearoa New Zealand**

3 Ery C. Hughes: Te Pū Ao | GNS Science (e.hughes@gns.cri.nz)

4 Sally Law: School of GeoSciences, University of Edinburgh (Sally.Law@ed.ac.uk)

5 Geoff Kilgour: Te Pū Ao | GNS Science (g.kilgour@gns.cri.nz)

6 Jon D. Blundy: University of Oxford (jonathan.blundy@earth.ox.ac.uk)

7 Heidi M. Mader: University of Bristol (h.m.mader@bristol.ac.uk)

8

9 This paper is a revised version of a non-peer review pre-print submitted to EarthArXiv, which  
10 has been submitted to the Journal of Volcanology and Geothermal Research special issue on  
11 the Okataina Volcanic Centre for peer review.

12

13 Twitter handles: @eryhughes, @sallylaw, @NZvolcanologist

14 **Storage, evolution, and mixing in basaltic eruptions from around the Okataina Volcanic**  
15 **Centre, Taupō Volcanic Zone, Aotearoa New Zealand**

16 Ery C. Hughes<sup>1,2,3\*</sup>, Sally Law<sup>4</sup>, Geoff Kilgour<sup>5</sup>, Jon D. Blundy<sup>6</sup>, and Heidy M. Mader<sup>1</sup>

17 1 School of Earth Sciences, University of Bristol, Wills Memorial Building, Queens Road,  
18 Bristol BS8 1RJ, UK

19 2 Division of Geological and Planetary Sciences, California Institute of Technology, Arms  
20 Laboratory, Pasadena, CA 91125, USA

21 3 Volcanology Team, National Isotope Centre/Avalon, Te Pū Ao | GNS Science, Lower Hutt,  
22 Aotearoa New Zealand

23 4 School of GeoSciences, University of Edinburgh, King's Buildings, Edinburgh EH9 3FE,  
24 UK

25 5 Volcanology Team, Wairakei Research Centre, Te Pū Ao | GNS Science, Taupō, Aotearoa  
26 New Zealand

27 6 Department of Earth Sciences, University of Oxford, South Parks Road, Oxford OX1 3AN,  
28 UK

29 \*Corresponding author. Email: [e.hughes@gns.cri.nz](mailto:e.hughes@gns.cri.nz)

30

31

### Abstract

32 The Okataina Volcanic Centre (OVC) is the most recently active caldera system in the Taupō  
33 Volcanic Zone, Aotearoa New Zealand. Although best known for its high rates of explosive  
34 rhyolitic volcanism, there are several examples of basaltic to basaltic-andesite contributions to  
35 OVC eruptions. These range from minor involvement of basalt in rhyolitic eruptions to the  
36 exclusively basaltic 1886 C.E. Plinian eruption of Tarawera. To explore the basaltic component  
37 supplying this dominantly rhyolitic area, we analyse the textures and compositions (minerals  
38 and melt inclusions) of four basaltic eruptions from within and around the OVC that have  
39 similar whole rock chemistry, namely: Terrace Rd, Rotomakariri, Rotokawau, and Tarawera.  
40 Data from these basaltic deposits provide constraints on the conditions of magma evolution  
41 and ascent in the crust prior to eruption, revealing that eruptions sample multiple distinct  
42 reservoirs during ascent to the surface. The most abundant basaltic component is generated by  
43 cooling-induced crystallisation of a common, oxidised, volatile-rich basaltic melt at various  
44 depths within the crust that mixes upon ascent. Despite similar bulk compositions, these four  
45 eruptions are texturally distinct as a result of their wide variation in eruption style.

46

47 **Keywords:** geochemistry, Tarawera, Terrace Rd, Rotomakariri, Rotokawau, melt inclusions

48

## 49 1 Introduction

50 Volcanic arcs are characterised by complicated sub-surface architectures that convert basaltic  
51 mantle-derived melt into a wide variety of more evolved arc magma compositions (e.g.,  
52 reviews by Ducea et al., 2015; Grove et al., 2012). Compositional variability can be derived  
53 from variations in the primary composition of the mantle melt input, extents of crustal  
54 assimilation, type of petrological processes occurring (e.g., crystallisation, degassing, mixing),  
55 and the conditions of magma stagnation (pressure, temperature). Static models that account for  
56 the evolution of melt composition in the crust are achieved through variations in temperature  
57 (e.g., Annen et al., 2006), whereas dynamic models drive compositional variation by reactive

58 melt percolation (e.g., Jackson et al., 2018); both mechanisms have been used to explain the  
59 compositional variability of arc magmas. Reconciling these models requires observations and  
60 analysis of volcanic rocks or exhumed crustal sections, which provide snapshots and time-  
61 integrated histories, respectively, of magmatic systems.

62 Both crustal and erupted materials at arcs are dominated by evolved magma compositions (i.e.,  
63 andesites to rhyolites) despite the large inputs of basaltic melt required for their formation.  
64 Most basalts never reach the surface due to relatively high magma density compared to the  
65 surrounding crust. Furthermore, these intrusions cool in the crust and either solidify to gabbroic  
66 plutons or generate more evolved magmas that separate and ascend to then erupt or cool to  
67 form felsic plutons. Periodic magma mixing (e.g., basalt with rhyolite) may be important in  
68 generating intermediate magmas and triggering eruptions (e.g., Laumonier et al., 2014; Sparks  
69 et al., 1977). Any basaltic magmas that do reach the surface will have traversed this  
70 complicated crustal region yet unravelling this cryptic differentiation history is not trivial and  
71 inevitably requires high resolution, *in situ* mineral analysis. Here, we utilise microanalytical  
72 geochemical methods to collect data on crystals and their melt inclusions to explore the paths  
73 taken by basaltic magmas beneath a dominantly rhyolitic caldera. We constrain how and where  
74 basaltic magmas are stored within the crust, and what petrological processes affect them. This  
75 is important for assessing the current state of magma reservoirs in the crust in the context of  
76 geophysical surveys and predicting potential precursory signals before a future eruption at  
77 caldera systems.

78 The Okataina Volcanic Centre (OVC) is one of two currently active caldera systems in the  
79 Taupō Volcanic Zone, Aotearoa New Zealand (Taupō Volcanic Centre, TVC, is the other).  
80 From several studies of the rhyolites, the sub-surface architecture below the OVC is known to  
81 comprise discrete rhyolitic melt-mush pockets that erupt compositionally distinct magmas  
82 within single eruptions (e.g., Cole et al., 2014; Sas et al., 2021; Shane et al., 2008a, 2007; Smith  
83 et al., 2004; Storm et al., 2011). Basaltic magmas are key to generating the more evolved  
84 magma compositions in the OVC, but little is known about their evolution. Heat and volatiles  
85 are assumed to be transferred between basalts and rhyolites to trigger rhyolitic eruptions (e.g.,  
86 Leonard et al. 2002; Shane et al. 2007, 2008; Smith et al. 2010), but the initial volatile contents  
87 of the basalts are largely unconstrained. Abundant evidence for basaltic-rhyolitic magma  
88 interaction also enables investigation of how magma mixing is related to basaltic eruption style  
89 (e.g., Leonard et al., 2002; Shane et al., 2005). In this study we combine textural observations  
90 with mineral and melt inclusion chemistries to constrain the magmatic compositions (including  
91 volatiles), conditions, and processes occurring during crustal storage and ascent of basaltic  
92 magmas around the OVC.

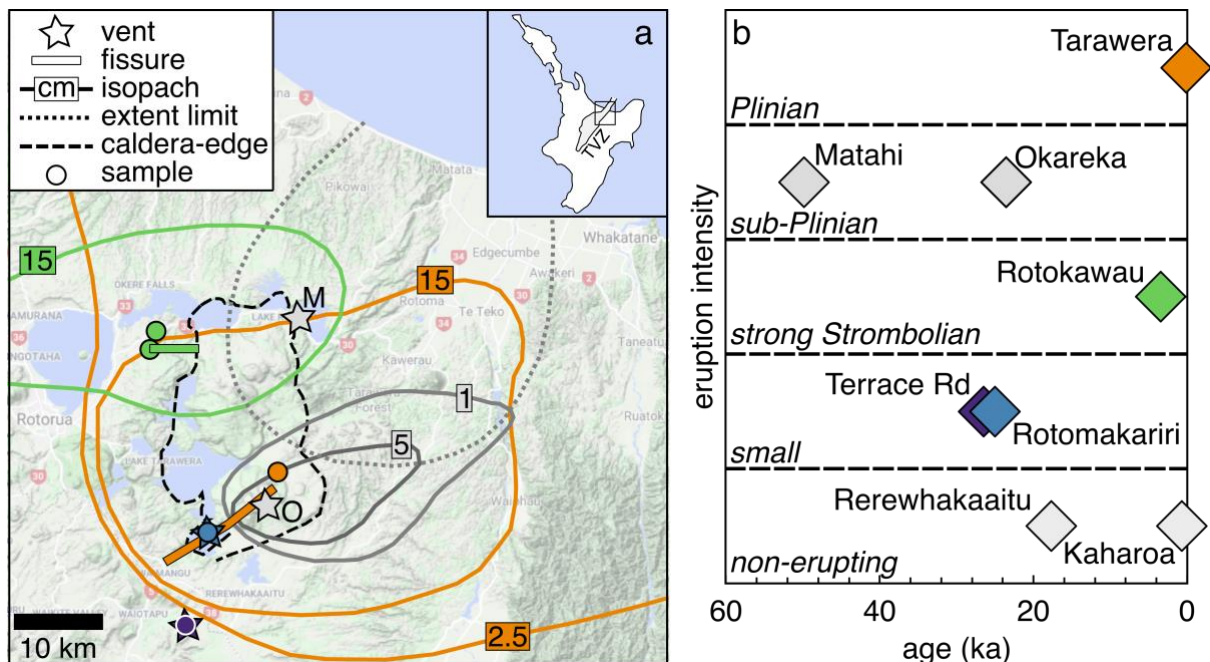
93

## 94 **2 Regional setting**

95 The Taupō Volcanic Zone (TVZ) is the most frequently active and productive silicic system  
96 on Earth (Wilson et al., 2009). Oblique subduction of the Pacific plate under continental  
97 Zealandia leads to the clockwise rotation of the eastern portion of the North Island, resulting  
98 in extension in the TVZ, crustal thinning, and basalt underplating (Houghton et al., 1995;  
99 Mortimer et al., 2017; Wilson et al., 1995). High rates of underplating drive the generation of  
100 voluminous silicic magma and, together with the relatively thin and faulted crust, enhance  
101 magma production and the rate of eruptions (e.g., Cole et al., 2014; Price et al., 2005).  
102 Extensive crustal contamination influences the isotopic composition of TVZ basalts and  
103 rhyolites (e.g., Gamble et al., 1993; Graham et al., 1995; Sas et al., 2021; Waight et al., 2017).

104 Basalts are volumetrically minor at the surface compared to andesites/dacites (ten times greater  
 105 in volume) and rhyolites (100 to 1000 times greater in volume) (Wilson et al., 1995). TVZ  
 106 basalts are classified as high-alumina and are generated by a combination of rift-induced  
 107 decompression melting and fluid-induced flux melting (Hiess et al., 2007; Law et al., 2021).  
 108 Active calderas have high inputs of basalt from the mantle wedge, which is caused by fluid-  
 109 fluxed melting of relatively fertile mantle (Barker et al., 2020; Zellmer et al., 2020). The mantle  
 110 source under these calderas is lherzolitic, as the sub-continental lithospheric mantle has been  
 111 removed by rifting and crustal thinning, shifting volcanism to rhyolitic rather than andesitic  
 112 (Law et al., 2021). Regions without active calderas have lower inputs of basalt due to either a  
 113 subdued influence from fluid-fluxing or a more depleted mantle source, plausibly caused by  
 114 prior melt extraction associated with formation of older calderas (Barker et al., 2020; Zellmer  
 115 et al., 2020). Basaltic eruptions throughout the TVZ are often associated with faults and  
 116 commonly erupt in association with rhyolitic magmas (Cole, 1970a; Hiess et al., 2007; Nairn  
 117 and Cole, 1981). Basaltic volcanism exhibits a wide range of eruption style, both within and  
 118 between individual eruptions and volcanic centres, and shallow conduit processes (including  
 119 interaction with external, non-magmatic water) are thought to play a major role in determining  
 120 eruption style (e.g., Carey et al., 2007; Houghton and Hackett, 1984).

121 The currently active OVC is overwhelmingly rhyolitic, but a diverse range of styles and  
 122 intensities of basaltic explosive activity is also present within and outside the caldera (Cole et  
 123 al., 2014; Nairn, 2002) (Figure 1a). Since ~55 ka there have been at least six basaltic eruptions  
 124 in this region, ranging from phreatomagmatic to magmatic and Strombolian to Plinian in  
 125 intensity (Table 1 and Figure 1) in addition to two examples of mafic enclaves and blebs in  
 126 exclusively rhyolitic eruptions (Cole et al., 2014; Nairn, 2002). Basaltic Plinian eruptions  
 127 are rare in the geological record, and Tarawera is the one of the most recent (Cole, 1970a; Nairn,  
 128 1979; Rowe et al., 2021; Thomas, 1888; Walker et al., 1984).



129  
 130 *Figure 1 (a)* Map of the region surrounding the Okataina Volcanic Centre (OVC), showing the caldera boundary  
 131 (black dashed curve); location of eruptive vents and fissures (coloured stars or lines; Beanland, 1989; Burt et al.,  
 132 1998; Darragh et al., 2006; Nairn, 2002, 1992); deposit thickness isopleths or extent limit (solid or dashed curves;  
 133 Beanland, 1989; Darragh et al., 2006; Nairn, 1992; Pullar and Nairn, 1972); and sample locations for this study  
 134 for the basaltic eruptions (circles). Colour indicates eruption as shown in (b) – eruptions analysed in this study are  
 135 in colour and other basalts from around the OVC are shown in grey. Inset shows the location of the main map and  
 136 the Taupō Volcanic Zone (TVZ, shaded area) in the North Island of Aotearoa New Zealand. M = Matahi, where

137 the dotted-grey line is the extent limit; and O = Okareka, where the solid-grey lines are the 1 and 5 cm isopachs.  
 138 **(b)** Qualitative eruption intensity against age (Buck et al., 2003; Hogg et al., 2003; Hopkins et al., 2021; Nairn,  
 139 2002; Newnham et al., 2003; Peti et al., 2021) for OVC basaltic magmas – Rerewhakaaitu and Kaharoa do not  
 140 appear in (a) because they only occur as basaltic enclaves and blebs within a rhyolitic eruption.

141 *Table 1* Basalts from around the Okataina Volcanic Centre (OVC) since the last caldera-forming eruption.

Eruption	Age (ka)	Description	DRE volume (km <sup>3</sup> ) [Column height (km)]
Tarawera*	1886 C.E.	Phreatomagmatic to magmatic, Strombolian to Plinian fissure <sup>1-3</sup>	0.25–0.48 <sup>4</sup> [~28] <sup>3</sup>
Kaharoa	0.6 <sup>5-6</sup>	Enclaves in rhyolitic eruption <sup>7-9</sup>	>0.01 <sup>9</sup>
Rotokawau*	3.44 ± 0.07 <sup>10</sup>	Phreatomagmatic (Surtseyan) and Strombolian fissure <sup>10-12</sup>	0.55 <sup>11</sup> [4.5–7] <sup>11</sup>
Rerewhakaaitu	17.6 <sup>13</sup>	Blebs in rhyolitic eruption <sup>14</sup>	n.d.
Okareka	23.5 <sup>15</sup>	Single vent, sub-Plinian phase prior to rhyolitic eruption <sup>16-17</sup>	0.01 <sup>16,18</sup>
Rotomakariri*	22–28 <sup>10</sup>	Single vent tuff cone <sup>10</sup>	n.d.
Terrace Rd*	25–28, 28 ± 2 <sup>10</sup>	Single vent (?), small phreatomagmatic <sup>10</sup>	n.d.
Matahi <sup>†</sup>	~45–55 <sup>19</sup>	Single vent, sub-Plinian <sup>20</sup>	<1 <sup>21</sup>

142 *Notes:* \*Eruptions analysed in this study. <sup>†</sup>The Matahi eruption occurred just prior to the Rotoiti Ignimbrite that  
 143 was the most recent OVC caldera-forming eruption. Volumes (DRE = dense rock equivalent) for Terrace Rd and  
 144 Rotomakariri are not determined (n.d.), but are likely small due to their limited occurrence (Nairn, 2002).  
 145 References: <sup>1</sup>Keam (1988), <sup>2</sup>Nairn and Cole (1981), <sup>3</sup>Walker et al. (1984), <sup>4</sup>Rowe et al. (2021), <sup>5</sup>Hogg et al. (2003),  
 146 <sup>6</sup>Buck et al. (2003) <sup>7</sup>Leonard et al. (2002), <sup>8</sup>Nairn et al. (2001), <sup>9</sup>Nairn et al. (2004), <sup>10</sup>Nairn (2002), <sup>11</sup>Beanland  
 147 (1989), <sup>12</sup>Beanland and Houghton (1978), <sup>13</sup>Newnham et al. (2003), <sup>14</sup>Shane et al., (2007), <sup>15</sup>Peti et al. (2021),  
 148 <sup>16</sup>Darragh et al. (2006), <sup>17</sup>Nairn (1992), <sup>18</sup>Shane et al. (2008a), <sup>19</sup>see discussion in Hopkins et al. (2021), <sup>20</sup>Pullar  
 149 and Nairn (1972), and <sup>21</sup>Froggatt and Lowe (1990).

150 Basaltic eruptions around the OVC are fed by dikes. Vents are often aligned along the main  
 151 NE-SW trending tectonic fabric, predominantly along the Tarawera Linear Vent Zone, but also  
 152 just outside the caldera boundaries (Nairn, 2002; Figure 1a). Most individual eruptions issued  
 153 from a single vent, but the Tarawera and Rotokawau eruptions occurred along fissures,  
 154 displaying a range of style and intensity both spatially and temporally within each eruption  
 155 (Nairn, 2002). For instance, the Tarawera eruption generated a ~17 km-long fissure, with  
 156 Strombolian to Plinian magmatic eruptions in the NE and phreatomagmatic eruptions in the  
 157 SW where it intersected an active hydrothermal system (Nairn, 1979; Nairn and Cole, 1981;  
 158 Rowe et al., 2021; Walker et al., 1984). The Tarawera fissure is broadly perpendicular to the  
 159 TVZ extension direction, in marked contrast to the E-W striking Rotokawau fissure (Beanland,  
 160 1989).

161 Many OVC rhyolitic eruptions are likely triggered by the injection of basaltic magmas (e.g.,  
 162 Leonard et al., 2002; Shane et al., 2008, 2007). Some rhyolitic eruptions were preceded by  
 163 basaltic eruptions, with either no (e.g., Matahi prior to Rotoiti) or direct (e.g., mixed basaltic-  
 164 rhyolitic clasts in Okareka) evidence for magma mixing prior to eruption, whereas others (e.g.,  
 165 Rerewhakaaitu and Kaharoa) host basaltic blebs and enclaves (e.g., Burt et al., 1998; Cole,  
 166 1973a; Cole et al., 2014; Leonard et al., 2002; Nairn, 1992; Pullar and Nairn, 1972; Schmitz  
 167 and Smith, 2004; Shane et al., 2007, 2008a). The OVC is passively degassing CO<sub>2</sub> and heat  
 168 today, and inferred basaltic dike intrusion events also occur, as well as evidence for cooling  
 169 intrusions (e.g., Benson et al., 2021; Hamling et al., 2022; Hughes et al., 2019b; Mazot et al.,  
 170 2014; Seward et al., 2022; Yang et al., in review).

171 All basalts (including blebs in rhyolitic eruptions) from around the OVC contain olivine,  
 172 clinopyroxene, and plagioclase crystals (sometimes in aggregates) within a glassy (e.g.,

173 Matahi) to highly microcrystalline groundmass (e.g., Cole, 1970b; Law et al., 2021; Nairn,  
174 2002, 1992; Rowe et al., 2021; Sable et al., 2009; Schmitz and Smith, 2004; Shane et al.,  
175 2008a). Additionally, most basalts contain entrained xenocrystic quartz and rhyolitic material  
176 (Beanland, 1989; Cole, 1973a; Nairn, 2002; Schmitz and Smith, 2004). Since ~55 ka in the  
177 OVC, hornblende has only been observed in basaltic enclaves in the Kaharoa eruption (Leonard  
178 et al., 2002). Clast vesicularity ranges from dense to highly vesicular, even within a single  
179 eruption (Beanland, 1989; Nairn, 2002; Shane et al., 2008a). Dense clasts are often used as  
180 evidence for interaction with external water (e.g., Beanland and Houghton, 1978; Carey et al.,  
181 2007).

182

### 183 **3 Methods**

184 We studied material from the Terrace Rd, Rotomakariri, Rotokawau, and Tarawera eruptions  
185 as they cover the full range of eruption styles and sizes (phreatomagmatic to magmatic and  
186 Strombolian to Plinian) observed around the OVC (Figure 1b). Rotomakariri and Tarawera  
187 occurred inside the caldera boundary (along one of the main linear vent zones), whereas  
188 Terrace Rd and Rotokawau occurred outside (Figure 1a). There are no published melt inclusion  
189 data for Terrace Rd, Rotomakariri, and Rotokawau, and only limited published data for  
190 Tarawera (Barker et al., 2020; Rowe et al., 2021); melt inclusions have been previously  
191 analysed from Okareka and Kaharoa (Barker et al. 2020).

192 To constrain pre-eruptive magmatic compositions, conditions, and processes, we analysed  
193 mineral and melt inclusion chemistry and textures. Scoria 4–8 mm in size were selected to  
194 ensure rapid clast cooling and Tarawera samples were collected off the volcano to avoid  
195 material that had cooled slowly. This increases the potential for glassy melt inclusions that  
196 retain their initial volatile content (Lloyd et al., 2013). Olivine, pyroxene, and plagioclase  
197 crystals were hand-picked from gently crushed clasts and either bulk mounted in epoxy or  
198 individually mounted and polished to expose a melt inclusion. Only naturally glassy  
199 clinopyroxene-hosted melt inclusions were analysed; no rehomogenisation experiments were  
200 carried out.

201 Olivine, pyroxene, and plagioclase were analysed using electron probe micro-analysis (EPMA)  
202 wavelength dispersive spectrometry (WDS). Unless otherwise stated, all analyses were taken  
203 from crystal cores. Melt inclusions from all eruptions were analysed using EPMA-WDS for  
204 major, minor, and volatile (S, Cl, and F) elements and for H<sub>2</sub>O using calibrated volatiles-by-  
205 difference (Hughes et al., 2019a). A subset of melt inclusions from Tarawera was analysed for  
206 H<sub>2</sub>O and CO<sub>2</sub> using secondary ion mass spectrometry (SIMS) prior to EPMA. To put mineral  
207 separate data into context, textural observations on thin sections were made using optical  
208 microscopy and scanning electron microscopy (SEM). Some mineral phases (and the  
209 groundmass glass for Rotomakariri) in the thin sections were analysed using semi-quantitative  
210 (sq) SEM energy dispersive spectroscopy (EDS) (sq-SEM-EDS) and EPMA-WDS to correlate  
211 the textures with mineral separates data.

212 To expand our dataset, we compiled mineral, melt inclusion, and whole rock data from the  
213 literature, particularly from basaltic eruptions not analysed in this study (e.g., Matahi, Okareka,  
214 Rerewhakaaitu, and Kaharoa). Several thermometers (melt, olivine-melt, clinopyroxene-melt,  
215 and clinopyroxene-orthopyroxene; Putirka, 2008), oxybarometers (melt Fe<sup>3+</sup>/Fe; Kress and  
216 Carmichael, 1991), and barometers (clinopyroxene-melt; Neave and Putirka, 2017, and H<sub>2</sub>O-  
217 CO<sub>2</sub> melt concentrations; Ghiorso and Gualda, 2015), as well as rhyolite-MELTS modelling  
218 (Ghiorso and Gualda, 2015; Gualda et al., 2012), were applied to mineral, melt inclusion, and  
219 whole rock data from this study and the literature. Data collection and reporting for melt

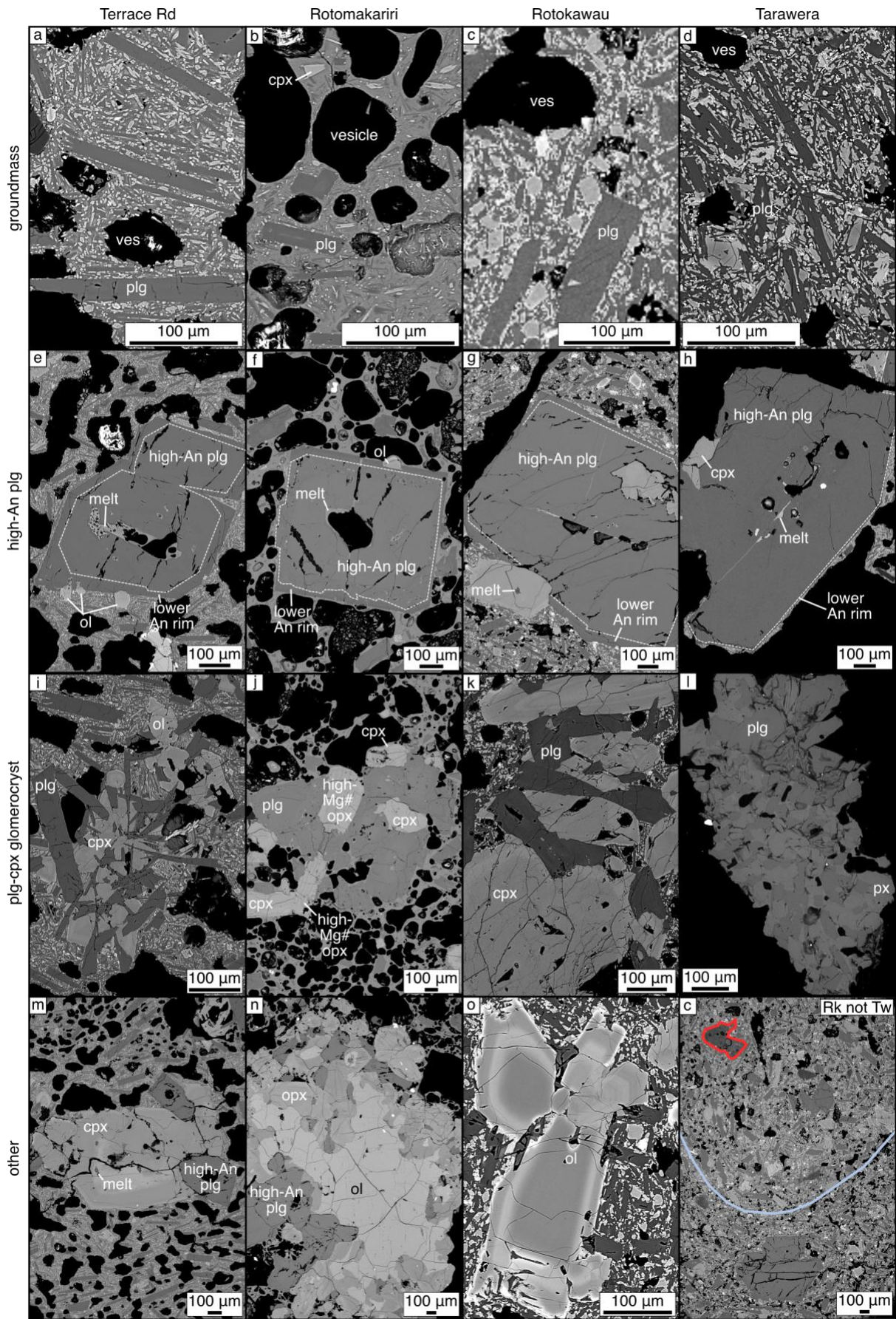
220 inclusions broadly follows the guidelines of Rose-Koga et al. (2021). Full analytical and  
221 calculation details, as well as all data collected and compiled, are provided in Supplementary  
222 Material.

223

## 224 **4 Textural and chemical characteristics**

### 225 *4.1 Vesicles, groundmass, and macrocrysts*

226 Texturally and chemically, Tarawera, Rotokawau, and Terrace Rd scoria are more similar to  
227 each other than to scoria from Rotomakariri. Tarawera, Rotokawau, and Terrace Rd are  
228 characterised by vesicles with complex shapes in a highly crypto- to microcrystalline  
229 groundmass containing olivine, clinopyroxene, plagioclase, and Fe-Ti oxide microlites (Figure  
230 2a, c, and d). Rotokawau and Tarawera scoria are homogeneously brown-to-black, whereas  
231 Terrace Rd is highly variable in colour (black to light-brown), including small domains (<3  
232 mm across) of black and grey material. At Terrace Rd, the groundmass is very similar in both  
233 the brown and black areas; Rotokawau also shows multiple groundmass textures, including  
234 flow alignment (Figure 2c). Rotomakariri scoria are homogeneously brown-to-black and have  
235 rounded vesicles in a groundmass of glass containing sparse microlites of plagioclase and  
236 clinopyroxene (Figure 2b). Further details are in Supplementary Material.



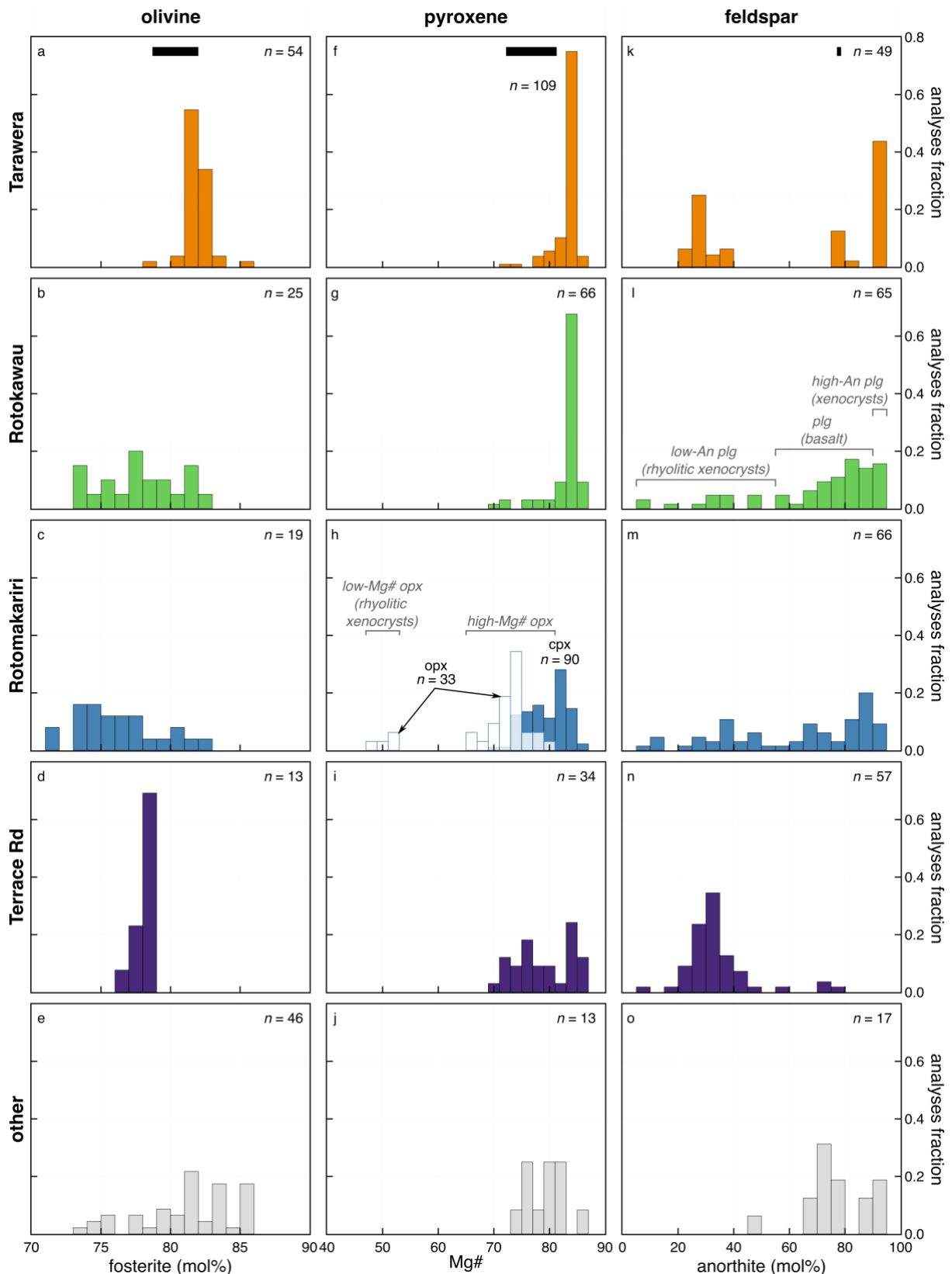
237  
238  
239

Figure 2 Annotated back-scattered electron (BSE) scanning electron microscope (SEM) images of scoria textures. Each column is a separate eruption: Terrace Rd (a, e, i, m), Rotomakariri (b, f, j, n), Rotokawau (c, g, k, o, and



240 additionally p at the bottom of the far-right column), and Tarawera (d, h, l). Different features are shown by row.  
241 **(a–d)** Groundmass textures, where in **(b)** plagioclase is An<sub>76</sub>. **(e–h)** High-An plagioclase (An<sub>93–96</sub> cores and An<sub>76–</sub>  
242 <sub>87</sub> rims) forms glomerocrysts with other phases. **(i–m)** Glomerocrysts of plagioclase and pyroxene: **(i)** plagioclase,  
243 clinopyroxene, and altered olivine on the edge; **(j)** plagioclase (core An<sub>83</sub>, rim An<sub>79</sub>), clinopyroxene (Mg# 75–78),  
244 and high-Mg# orthopyroxene (Mg# = 71 core, 75 rim); **(k)** clinopyroxene (Mg# 85) and plagioclase (An<sub>88</sub>); **(l)**  
245 intergrown plagioclase and pyroxene; **(m)** high-An plagioclase and olivine (Fo<sub>76</sub>) attached to a clinopyroxene  
246 (Mg# = 65 core, 80 middle, 73 rim). **(n–p)** Other textures: **(n)** glomerocryst: centre is a partially resorbed olivine  
247 (Fo<sub>83</sub>), with overgrowths of high-Mg# orthopyroxene (Mg# 76), high-An plagioclase (An<sub>92</sub> core, An<sub>85</sub> rim), and  
248 some clinopyroxene on the outer portion; **(o)** olivine macrocryst (dark portions Fo<sub>80</sub>, bright band Fo<sub>75</sub>); and **(p)**  
249 alignment of plagioclase from basalt-basalt mixing (blue line) and region of evolved material is outlined in red.  
250 *Abbreviations:* ves = vesicle, ol = olivine, plg = plagioclase, cpx = clinopyroxene, opx = orthopyroxene, and px  
251 = pyroxene.

252 Terrace Rd, Rotokawau, and Rotomakariri contain abundant macrocrysts, mostly as  
253 glomerocrysts (Figure 2i–n), whereas Tarawera is almost macrocryst- and glomerocryst-free  
254 (see also Law et al., 2021). All eruptions have a similar mineralogy of olivine, plagioclase, and  
255 clinopyroxene, with Rotomakariri additionally containing abundant orthopyroxene. Alkali  
256 feldspars and quartz were found in all eruptions. Olivine composition varies between eruptions,  
257 with a narrow range in molar forsterite (Fo) content at Terrace Rd (Fo<sub>76–79</sub>) and Tarawera (Fo<sub>79–</sub>  
258 <sub>85</sub>) and a wide range at Rotomakariri (Fo<sub>71–82</sub>) and Rotokawau (Fo<sub>73–82</sub>) (Figure 3a–e).  
259 Groundmass olivine from Tarawera analysed by Rowe et al. (2021) has similar Fo to the  
260 macrocrysts (Figure 3a). Clinopyroxene composition is similar across all eruptions, including  
261 groundmass clinopyroxene from Tarawera reported by Rowe et al. (2021), with Mg# 69–87  
262 (Figure 3f–k). Orthopyroxene from Rotomakariri is bimodal in composition (Figure 3h). High-  
263 Mg# orthopyroxene (83–87) is found as macrocrysts in Rotomakariri (and rarely Rotokawau  
264 and Tarawera) and sometimes as inclusions in clinopyroxene at Terrace Rd and Rotokawau.  
265 Low-Mg# orthopyroxene (67–83), sometimes with inclusions of apatite, occurs in all eruptions.  
266 Plagioclase displays a wide range of molar anorthite content (Figure 3k–o). Some “high-An”  
267 plagioclase grains have very calcic (>An<sub>90</sub>) cores with coarse sieving and normal zoning to a  
268 thin, unsieved, less calcic rim (Figure 2e–h). At Terrace Rd, >An<sub>90</sub> was not measured via  
269 EPMA on picked grains from but was observed in SEM images (e.g., Figure 2e). Many  
270 plagioclase crystals have lower An (55–90), are mostly unzoned, and occur as both macrocrysts  
271 and inclusions in clinopyroxene at Terrace Rd, in low-Mg# orthopyroxene at Rotokawau, and  
272 in both clinopyroxene and orthopyroxene at Rotomakariri. This plagioclase composition is  
273 similar to rims on the highly calcic plagioclase and plagioclase microlites in the Tarawera  
274 groundmass (Rowe et al., 2021). For plagioclase with >An<sub>55</sub>, FeO content is high (>0.4 wt%)  
275 and decreases with increasing An (see Figure S6 in Supplementary Material). There are some  
276 “low-An”, texturally variable plagioclases with An<sub><55</sub> and FeO <0.4 wt%. Unlike mineral  
277 compositions, which are similar across different eruptions, glomerocrysts are unique to  
278 individual eruptions. More detailed descriptions of both the minerals and glomerocrysts are  
279 provided in Supplementary Material.



280  
 281  
 282  
 283  
 284  
 285  
 286  
 287

Figure 3 Histograms of mineral chemistry showing fraction of crystal core analyses in each compositional bin (number of analyses  $n$  indicated for each panel). Each column represents a different mineral phase, labelled along the top: (a–e) olivine – forsterite content, (f–j) pyroxene – Mg# (filled bars are for cpx, unfilled bars in (h) are for opx, with different opx populations labelled in grey), and (k–o) plagioclase – anorthite content (different plg populations are labelled in grey in (l) but apply to all eruptions). Each row represents an individual eruption, which are labelled down the left-hand side and shown using colour: (a, f, k) Tarawera (orange), (b, g, l) Rotokawau (green), (c, h, m) Rotomakariri (blue), (d, i, n) Terrace Rd (purple), and (e, j, o) other OVC basalts (grey), which

288 includes Kaharoa, Rerewhakaaitu, Okareka, and Matahi. Range of microlite compositions from Rowe et al. (2021)  
289 for Tarawera shown as black bars in (a, f, k). *Data sources*: Matahi (Davis, 1985); Terrace Rd (Law et al., 2021;  
290 this study); Rotomakariri (Law et al., 2021; this study); Okareka (Barker et al., 2020; Shane et al., 2008a);  
291 Rerewhakaaitu (Shane et al., 2007), Rotokawau (Beanland, 1989; Hiess et al., 2007; Law et al., 2021; this study);  
292 Kaharoa (Barker et al., 2020; Leonard et al., 2002), Tarawera (Barker et al., 2020; Hiess et al., 2007; Law et al.,  
293 2021; Rowe et al., 2021; this study).

294

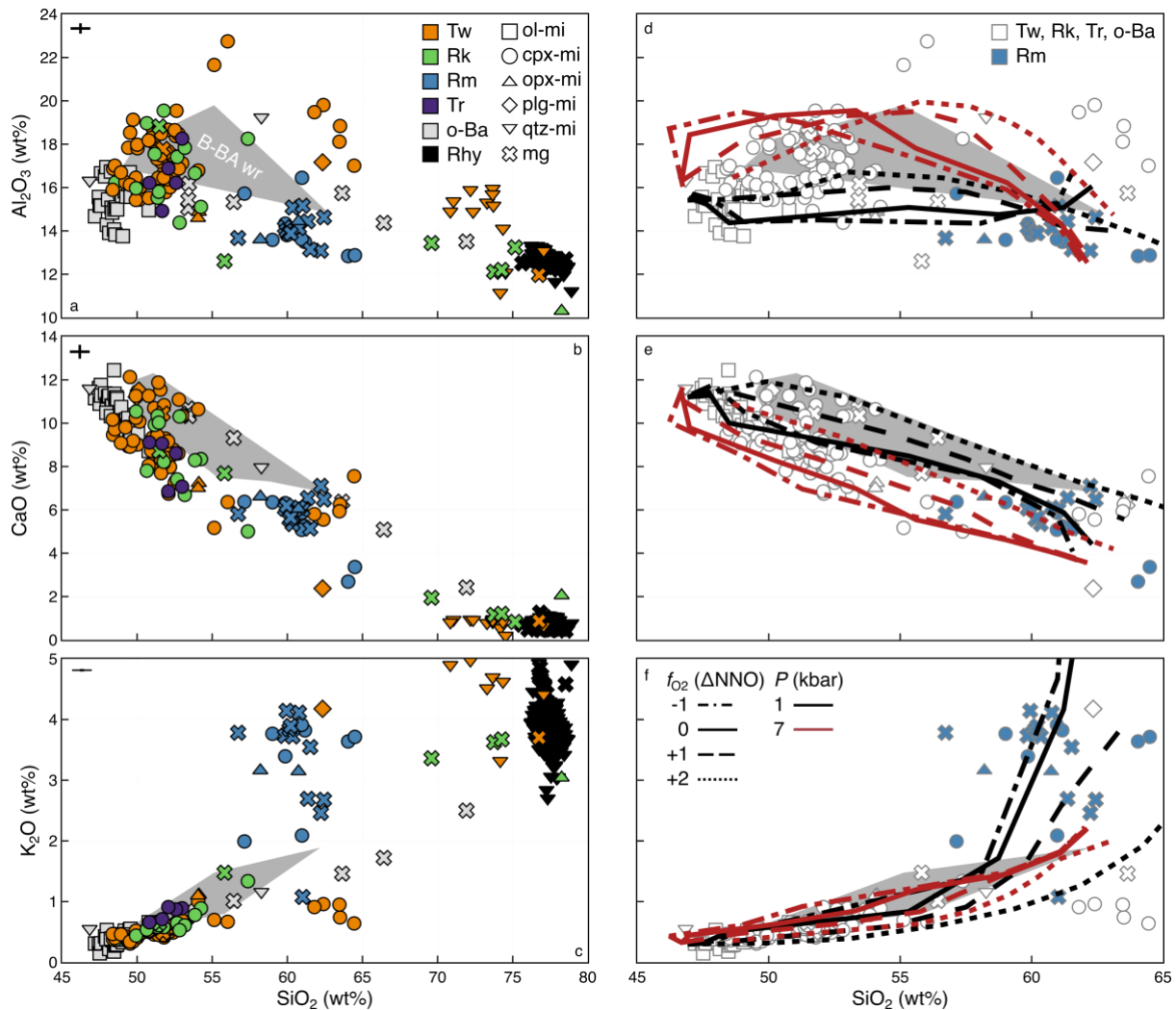
#### 295 4.2 Melt inclusions

296 Most glass analyses in this study come from melt inclusions hosted in clinopyroxene, with  
297 minor orthopyroxene-hosted melt inclusion and groundmass glass analyses (Figure 4 and  
298 Figure 5; additional data are shown in Figure S7 of Supplementary Material). From our study,  
299 most glass analyses are from Tarawera, followed by Rotokawau then Rotomakariri, with a  
300 small number from Terrace Rd. The Tarawera dataset is supplemented with melt inclusion data  
301 from Barker et al. (2020) and Rowe et al. (2021).

302 Crystallisation, diffusion, and bubble-formation can alter major and volatile element chemistry  
303 of melt inclusions after entrapment (e.g., Barth et al., 2019; Barth and Plank, 2021; Bucholz et  
304 al., 2013; Danyushevsky et al., 2000, 1988; Dungan and Rhodes, 1978; Gaetani et al., 2012;  
305 Gaetani and Watson, 2002, 2000; Hartley et al., 2014, 2015; Lowenstern, 2003, 1995; Moore  
306 et al., 2015; Nielsen et al., 1998; Rasmussen et al., 2020; Roedder, 1979; Saper and Stolper,  
307 2020; Schiano, 2003; Sobolev and Shimizu, 1993; Wallace et al., 2015). Based on mineral-  
308 melt exchange equilibria, most melt inclusions were not in equilibrium with their host crystal  
309 indicating post-entrapment crystallisation (PEC) has occurred (Figure S3a in Supplementary  
310 Material). The effects of PEC were corrected for using the method of Collins et al. (2022) and  
311 only data with <|15|% PEC-correction were used (see Supplementary Material for details).

312 Only the glass composition of melt inclusions was analysed; there was no attempt to account  
313 for volatiles contained in co-existing vapour bubbles (i.e., composition and size of vapour  
314 bubbles were not measured) to reconstruct bulk melt inclusion compositions. CO<sub>2</sub> is greatly  
315 affected by bubble formation, whilst H<sub>2</sub>O, S, and Cl are less affected due to lower partitioning  
316 into the vapour phase and/or potential kinetic effects (e.g., Hartley et al., 2014; MacLennan,  
317 2017; Moore et al., 2015; Rasmussen et al., 2020; Wallace et al., 2015). Rather than add  
318 additional uncertainty related to reconstructing the original melt composition, we assume CO<sub>2</sub>  
319 concentrations represent minimum estimates of the CO<sub>2</sub> content of the melt, and do not try and  
320 fit degassing trends to our data. Bulk (i.e., melt + bubble) H<sub>2</sub>O content can additionally be  
321 altered by diffusion into or out of the melt inclusion, which is discussed below (e.g., Barth et  
322 al., 2019; Barth and Plank, 2021; Bucholz et al., 2013; Gaetani et al., 2012; Hartley et al., 2015,  
323 2014).

324 Melt inclusions and matrix glasses show a considerable range in composition (Figure 4a–c).  
325 Terrace Rd, Rotokawau, and Tarawera melt inclusions are predominantly basaltic to basaltic-  
326 andesite in composition, whereas Rotomakariri melt inclusions and matrix glasses range from  
327 basaltic andesite to dacitic (mostly andesitic). There are a small number of andesite-dacite melt  
328 inclusions from Tarawera and some matrix glass data from Tarawera and Rotokawau that are  
329 dacite-rhyolite. Basaltic to basaltic-andesite melt inclusions are similar in Terrace Rd,  
330 Rotokawau, and Tarawera, but were not found in Rotomakariri (Figure 4a–c). The most  
331 basaltic of these melt inclusions overlap with the higher SiO<sub>2</sub> range of the olivine-hosted melt  
332 inclusions from Barker et al. (2020) and some of these melt inclusions overlap with whole rock  
333 data (Figure 4a–c). There is a wide-range of Al<sub>2</sub>O<sub>3</sub> at a given SiO<sub>2</sub> (15–19 wt% Al<sub>2</sub>O<sub>3</sub> at 50  
334 wt% SiO<sub>2</sub>; Figure 4a). CaO decreases with increasing SiO<sub>2</sub>, with some melt inclusions having  
335 higher CaO at a given SiO<sub>2</sub>, overlapping with the whole rock data (Figure 4b). K<sub>2</sub>O increases  
336 with SiO<sub>2</sub> for both melt inclusions and whole rocks (Figure 4c).

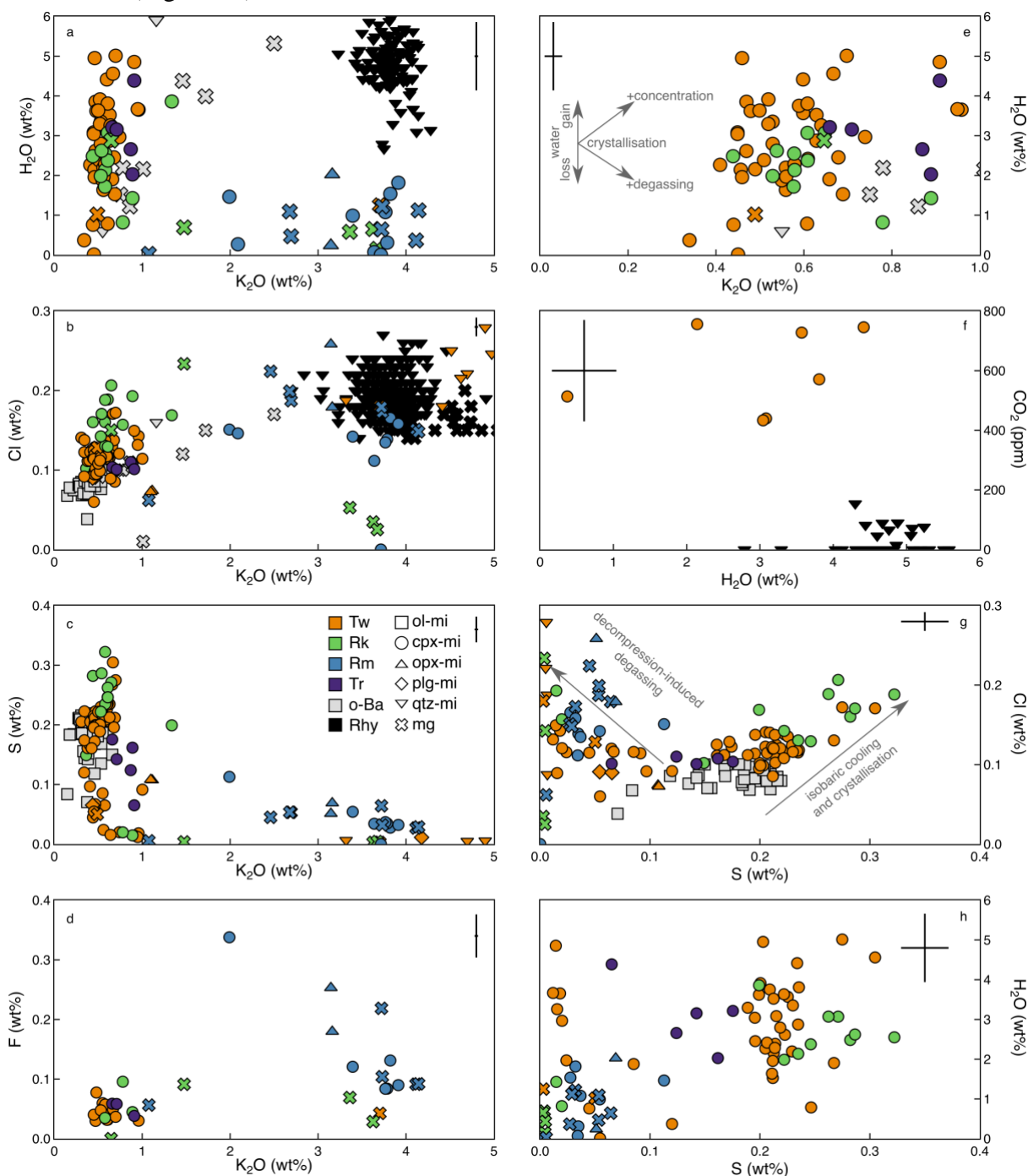


337

338 *Figure 4* Major element systematics for melt composition data for (a)  $\text{Al}_2\text{O}_3$ , (b)  $\text{CaO}$ , and (c)  $\text{K}_2\text{O}$  vs.  $\text{SiO}_2$ .  
 339 Symbol shapes distinguish between melt inclusion (PEC-corrected, hosted in olivine = square, clinopyroxene =  
 340 circle, plagioclase = diamond, orthopyroxene = up-triangle, or quartz = down-triangle) and groundmass glass  
 341 (cross). Different eruptions are indicated by symbol colour (Tarawera – Tw = orange, Rotokawau – Rk = green,  
 342 Rotomakariri – Rm = blue, Terrace Rd – Tr = purple, other OVC basalts – o-Ba = grey, and OVC rhyolites – Rhy  
 343 = black). The range in composition for whole rock data for basalt to basaltic-andesite OVC eruptions is shown by  
 344 a grey field labelled “B-BA wr”. Uncertainties for our data are indicated in the top-left corner of each panel and  
 345 are two standard deviations of the precision based on repeat analyses of VG-2 over all analytical sessions (note  
 346 the  $\text{K}_2\text{O}$  error bar is small). In (d–f) the results from Rhyolite-MELTS modelling (note the reduced range of  $\text{SiO}_2$   
 347 on the x-axis) is overlain on the melt data (white symbols with grey outlines are all data shown in (a–c) except  
 348 Rotomakariri, which is shown in blue, and the whole rock data in the grey region). Calculations are from 1300 to  
 349 900 °C, 1 wt %  $\text{H}_2\text{O}$  and 1000 ppm  $\text{CO}_2$ , 1 (black) or 7 (red) kbar, and various oxygen fugacity ( $f_{\text{O}_2}$ :  $\Delta\text{NNO}$ -1  
 350 dot-dash, 0 solid, +1 dash, and +2 dot) from a single melt composition. Additional data and results are shown in  
 351 Figure S7 and S8 of Supplementary Material. *Data sources*: melt inclusion and groundmass glass for Terrace  
 352 Road, Rotomakariri, and Rotokawau (this study); Tarawera melt inclusions hosted in clinopyroxene (this study;  
 353 Rowe et al., 2021), olivine (Barker et al., 2020), plagioclase, orthopyroxene and quartz (Rowe et al., 2021);  
 354 olivine-hosted melt inclusions for Okareka and Kaharoa (Barker et al., 2020); glass analyses from mafic blebs  
 355 from Rerewhakaaitu (Shane et al., 2007); OVC basaltic whole rock (Beanland, 1989; Bowyer, 2001; Cole, 1979,  
 356 1973b; Gamble et al., 1993, 1990; Grange, 1937; Hiess et al., 2007; Leonard et al., 2002; Nairn, 1992, 1981, 1979;  
 357 Nairn et al., 2004; Nairn, 2002; Pittari et al., 2016; Rooney and Deering, 2014; Rowe et al., 2021; Schmitz and  
 358 Smith, 2004; Shane et al., 2008a; Zellmer et al., 2020); and OVC rhyolitic melt inclusions and matrix glass  
 359 (Johnson et al., 2011).

360 Basaltic to basaltic-andesite melt inclusions from Tarawera have a wide range in  $\text{H}_2\text{O}$  contents  
 361 (0–5 wt%), whereas Terrace Rd (2.0–4.4 wt%) and Rotokawau (0.8–3.1 wt%) have a more  
 362 limited range (Figure 5a and e). The lack of correlation between  $\text{H}_2\text{O}$  and  $\text{K}_2\text{O}$  suggests

363 crystallisation has been overprinted by diffusive water-loss and hence H<sub>2</sub>O contents are a  
 364 a minimum (Figure 5e). Chlorine concentrations are lowest for Terrace Rd (~1000–1100 ppm),  
 365 then Tarawera (~850–1700 ppm); Rotokawau has the highest (~1300–2300 ppm), which  
 366 positively correlates with K<sub>2</sub>O (Figure 5b). Sulfur has a similarly wide range in all three  
 367 eruptions (~30–3300; Figure 5c) and fluorine concentrations are also similar (~30–1000;  
 368 Figure 5d), neither of which correlate with K<sub>2</sub>O. CO<sub>2</sub> (433–756 ppm) was measured for a subset  
 369 of Tarawera melt inclusions only (Figure 5f). For S > 1000 ppm, S and Cl positively correlate,  
 370 whereas for S < 1000 ppm they negatively correlate (Figure 5g); S and H<sub>2</sub>O show broad  
 371 correlation (Figure 5h).



372  
 373 *Figure 5* Volatiles systematics for melt composition data for: (a) H<sub>2</sub>O, (b) Cl, (c) S, (d) F, and (e) H<sub>2</sub>O (zoomed  
 374 in scale compared to a) vs. K<sub>2</sub>O; (f) CO<sub>2</sub> vs. H<sub>2</sub>O; and (g) Cl and (h) H<sub>2</sub>O vs. S. Symbol shapes distinguish between  
 375 melt inclusion (PEC-corrected, hosted in olivine = square, clinopyroxene = circle, plagioclase = diamond,  
 376 orthopyroxene = up-triangle, or quartz = down-triangle) and groundmass glass (cross). Different eruptions are

377 indicated by symbol colour (Tarawera – Tw = orange, Rotokawau – Rk = green, Rotomakariri – Rm = blue,  
378 Terrace Rd – Tr = purple, other OVC basalts – o-Ba = grey, and OVC rhyolites – Rhy = black). Uncertainties for  
379 our data are indicated in each panel as two standard deviations of precision based on repeat analyses of VG-2 over  
380 all analytical sessions for EPMA data (note the K<sub>2</sub>O error bar is small) or two standard deviations of the minimum  
381 precision based on repeat analyses of standards over all analytical sessions for SIMS data in (f). Trends for  
382 different processes are shown with grey arrows and labelled in (e) and (f). *Data sources*: melt inclusion and  
383 groundmass glass for Terrace Road, Rotomakariri, and Rotokawau (this study); Tarawera melt inclusions hosted  
384 in clinopyroxene (this study; Rowe et al., 2021), olivine (Barker et al., 2020), plagioclase, orthopyroxene and  
385 quartz (Rowe et al., 2021); olivine-hosted melt inclusions for Okareka and Kaharoa (Barker et al., 2020); glass  
386 analyses from mafic blebs from Rerewhakaaitu (Shane et al., 2007); and melt inclusions and groundmass glass  
387 from OVC rhyolites (Johnson et al., 2011).

388 Rotomakariri melt inclusions and groundmass glass are mostly andesitic, with low CaO and  
389 Al<sub>2</sub>O<sub>3</sub> and high K<sub>2</sub>O (Figure 4a–c). H<sub>2</sub>O and S are lower than most of the basaltic to basaltic-  
390 andesite melt inclusions, although similar to the low-sulfur (S <1000 ppm) set of  
391 clinopyroxene-hosted melt inclusions (Figure 5a and c). Chlorine is high and similar to  
392 Rotokawau (Figure 5b); fluorine is much higher than any of the basalts (Figure 5d). At  
393 Tarawera, a few clinopyroxene-hosted melt inclusions are also andesite-dacite, but have higher  
394 Al<sub>2</sub>O<sub>3</sub>, similar CaO, and lower K<sub>2</sub>O than Rotomakariri melt inclusions (Figure 4a–c). Dacite-  
395 rhyolite melt inclusions and groundmass glass are associated with orthopyroxene and quartz  
396 from Rotokawau and Tarawera (Figure 4a–c) and have low H<sub>2</sub>O, variable Cl, very low S, and  
397 low F (Figure 5a–d).

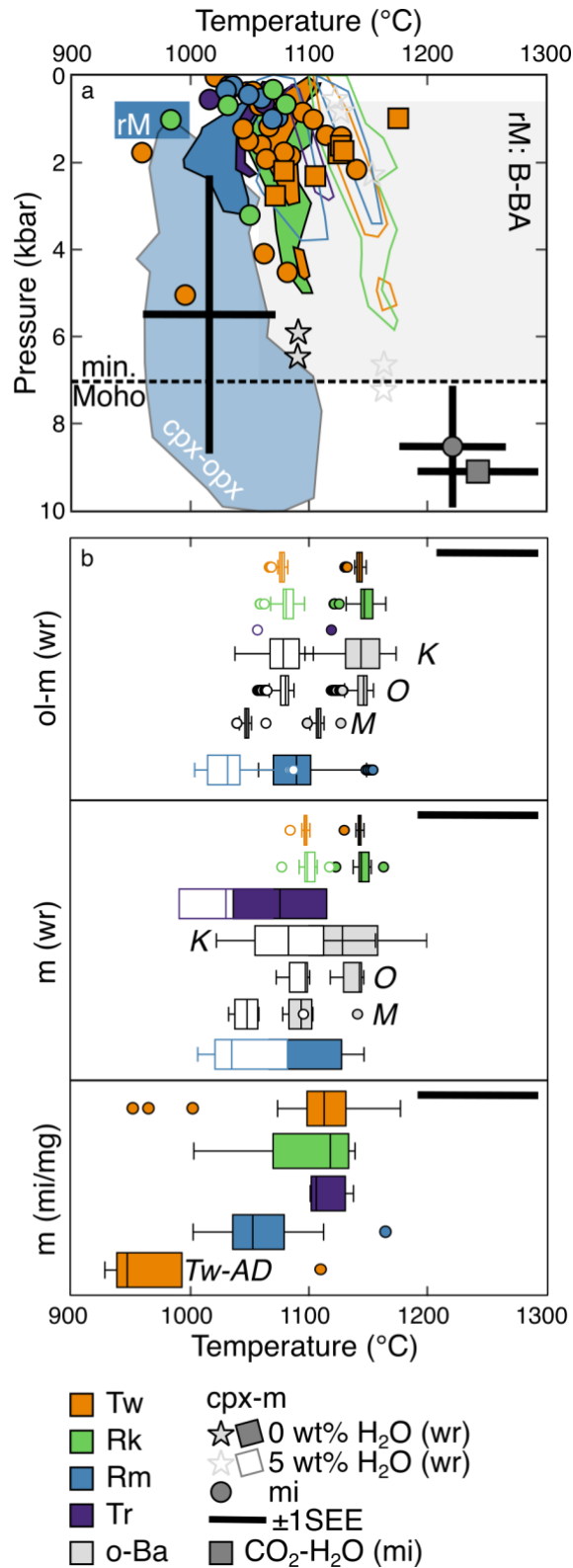
398

## 399 **5 Pre- and syn-eruptive storage, evolution, and mixing of multiple magmas**

### 400 *5.1 Similar basalts erupted in Tarawera, Terrace Rd, and Rotokawau*

#### 401 5.1.1 Polybaric crystallisation and mixing

402 Most of the mineral and melt inclusion analyses in this study, namely clinopyroxene and their  
403 melt inclusions, An<sub>50–90</sub> plagioclase, and groundmass material (except for Rotomakariri) were  
404 derived from basaltic magma (Figure 3 and Figure 4). Olivine compositions indicate these melts  
405 are not mantle-derived, but have already undergone prior crystallisation (Law et al., 2021). The  
406 spread in temperatures inferred from thermometry (Figure 6) suggests cooling-induced  
407 crystallisation is responsible for the compositional range of whole rock and melt inclusion data.  
408 The narrower spread in compositions and temperatures for whole rock and minerals compared  
409 to melt inclusions is consistent with the basaltic composition of the system. Conversely, melt  
410 inclusion compositions reflect local changes in temperature and associated crystallisation,  
411 recording snapshots of the melt present in a crystal-rich magma reservoir at depth. The mushy  
412 nature of this reservoir is further evidenced by abundant glomerocrysts in Terrace Rd,  
413 Rotomakariri, and Rotokawau (Figure 2i–n).



414

415 *Figure 6* Pressure and temperature estimates for each eruption (shown by colour, other OVC basalts include  
 416 Kaharoa – K, Okareka – O, and Matahi – M). (a) Pressure vs. temperature from: cpx-m using whole rock data  
 417 (coloured outlines are assuming 0 wt% H<sub>2</sub>O and filled regions are 5 wt%) and melt inclusion data (circles), where  
 418 the standard errors of estimate (SEE) is shown in the bottom-right corner by the thick black lines with a circle in  
 419 the middle; cpx-opx (labelled cpx-opx), where the SEE is shown by the thick black lines in the region; melt  
 420 inclusion CO<sub>2</sub>-H<sub>2</sub>O for minimum P and melt composition for T (squares), where the SEE is shown in the  
 421 bottom-right corner by the thick black line with a square in the middle; and Rhyolite-MELTS modelling (regions labelled  
 422 rM and rM: B-BA). Minimum depth of the TVZ Moho (Bannister et al., 2004) indicated by dashed black horizontal

423 line. **(b)** Box and whisker plots for temperature using ol-m and whole rock/melt inclusion/matrix glass  
424 composition. Estimates using whole rock compositions are shown assuming a melt composition that is anhydrous  
425 (filled) or H<sub>2</sub>O-saturated ( $\leq 5$  wt%, unfilled); measured H<sub>2</sub>O content is used for melt inclusions. The edges of the  
426 “box” are at the 1<sup>st</sup> and 3<sup>rd</sup> quartile of the data, with the median indicated by a horizontal line within the box. The  
427 “whiskers” extend out to the minimum and maximum data points within  $1.5\times$  the interquartile range (range  
428 between 1<sup>st</sup> and 2<sup>nd</sup> quartile) beyond the 1<sup>st</sup> and 3<sup>rd</sup> quartiles. Any outliers outside the whiskers are shown as  
429 individual data points (circles). The SEE for each thermometer is shown by the thick black line in the top-right of  
430 each panel. *Abbreviations*: ol = olivine, m = melt, wr = whole rock, cpx = clinopyroxene, mi = melt inclusion, and  
431 opx = orthopyroxene. Full descriptions of calculations given in Supplementary Material.

432 A wide range of pressures ( $\sim 7$  kbar to surface) is derived from melt-clinopyroxene barometry,  
433 with most estimates less than 3 kbar (Figure 6a). Based on volatile solubility, the H<sub>2</sub>O-CO<sub>2</sub>  
434 measurements require some melts to be derived from at least 3 kbar (Figure 6a). These estimates  
435 overlap with pressure-temperature estimates for Tarawera from Rowe et al. (2021). The high  
436 Al<sub>2</sub>O<sub>3</sub> requires plagioclase crystallisation to have been suppressed, suggesting differentiation  
437 at higher pressures (e.g., Blatter et al., 2013; Marxer et al., 2021; Müntener and Ulmer, 2018a;  
438 Nandedkar et al., 2014). Rhyolite-MELTS modelling is used to show that the compositions of  
439 melt inclusion and whole rock data do not correspond to fractional crystallisation at a unique  
440 pressure and oxygen fugacity (Figure 4d–f). Instead, the range in melt compositions is  
441 bracketed by fractional crystallisation during cooling (to 1050 °C) from a common, H<sub>2</sub>O-  
442 saturated parent melt at relatively oxidised ( $\Delta\text{NNO}=0$  to +2) conditions at pressures between 1  
443 and 7 kbar (Figure 4d–f and “rM: B-BA” region in Figure 6a). The oxygen fugacity range from  
444 Rhyolite-MELTS agrees with the limited literature whole rock Fe<sup>3+</sup>/Fe<sub>T</sub> data, which imply  
445 relatively oxidised conditions ( $\sim\Delta\text{NNO}+1$ ). Together these observations imply polybaric  
446 crystallisation of a single composition of basaltic magma (Figure 6a). Given the large model  
447 uncertainties (e.g.,  $\pm 1.4$  kbar for cpx-melt barometry; Putirka, 2008), individual magma  
448 reservoirs cannot be distinguished. However, the detailed mineral compositions (e.g., olivine;  
449 Figure 3a–e) and glomerocryst textures are distinct between eruptions (Figure 2i–n) indicating  
450 evolution in discrete, isolated pods prior to eruption, consistent with their known temporal and  
451 spatial spread.

452 The range in major element composition at a single SiO<sub>2</sub> (especially obvious in Al<sub>2</sub>O<sub>3</sub>; Figure  
453 4d) is then a result of mixing between these basaltic magmas and their differentiated products.  
454 Interaction between basaltic magmas is also evidenced by the textures in the scoria, which  
455 indicate mixing between different batches of basalt with subtly different crystallisation  
456 conditions (i.e., come from different places in the magmatic system) or decompression histories  
457 (e.g.,  $T$ -H<sub>2</sub>O conditions). At Tarawera, this includes the melt represented by the macrocryst-  
458 poor whole rock composition and the low/high-S melt inclusions (Figure 5g). A similar picture  
459 applies to Rotokawau, where mingled groundmass textures suggest multiple basaltic melts  
460 (Figure 2c). For Terrace Rd, the small glomerocrysts could be phenocrystic or antecrystic,  
461 whereas the large glomerocrysts are antecrystic and there is evidence for multiple melts in the  
462 groundmass (Figure 2e, i, and m). We interpret these observations in terms of evolution of a  
463 single, primitive, oxidised basalt magma in distinct, isolated, mushy pods due primarily to  
464 cooling-induced crystallisation, with some additional degassing and mixing during ascent of  
465 discrete magma batches.

466

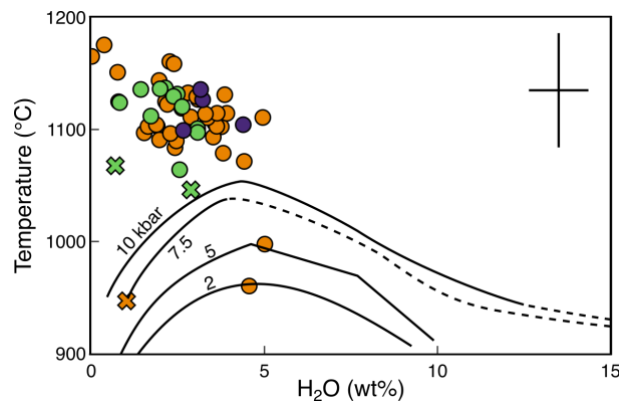
### 467 5.1.2 Volatiles contents and processes

468 H<sub>2</sub>O and CO<sub>2</sub> data are scattered, reflecting post-entrapment processes overprinting original  
469 magmatic conditions, such as bubble formation reducing CO<sub>2</sub> concentrations and H-diffusion  
470 modifying H<sub>2</sub>O (e.g., Barth et al., 2019; Barth and Plank, 2021; Bucholz et al., 2013; Gaetani  
471 et al., 2012; Hartley et al., 2015, 2014; Maclennan, 2017; Moore et al., 2015; Rasmussen et al.,



472 2020; Wallace et al., 2015) (Figure 5a, e, and f). The highest measured concentrations are ~5  
473 wt% H<sub>2</sub>O and ~750 ppm CO<sub>2</sub>, reflecting lower bounds on the H<sub>2</sub>O-CO<sub>2</sub> concentrations of the  
474 magma. Measured water contents overlap with inferred melt water contents from melt  
475 inclusions and clinopyroxene H contents from Rowe et al. (2021).

476 Amphibole was not observed in the eruptions studied here. Amphibole has been described only  
477 in the groundmass of basaltic and gabbroic enclaves from the Kaharoa eruption, where  
478 amphibole crystallisation is thought to have been triggered by a late-stage increase in H<sub>2</sub>O,  
479 possibly due to interaction with rhyolite (Leonard et al., 2002). Most of the melt inclusions at  
480 Tarawera, Rotokawau, and Terrace Rd record temperatures that are too high (>1050 °C) for  
481 amphibole stability despite their relatively high H<sub>2</sub>O concentrations (Figure 7) (Foden and  
482 Green, 1992). This suggests that basalt-rhyolite mixing prior to the Kaharoa eruption moved  
483 the magma into the amphibole stability field by cooling, rather than by increasing its H<sub>2</sub>O  
484 content.



485  
486 *Figure 7* Temperature vs. H<sub>2</sub>O for melt inclusion data (see Figure 4 for interpretation of the symbol shape and  
487 colour – only PEC-corrected data from this study are plotted). Temperature is derived from the melt composition  
488 and measured H<sub>2</sub>O concentration is plotted. Black curves are maximum temperatures amphibole is stable for a  
489 given H<sub>2</sub>O content of the system from Foden and Green (1992) for different pressures (written on each line).  
490 Uncertainties are indicated for  $T$  ( $\pm 1$ SEE) and H<sub>2</sub>O ( $\pm 2$  sd of the precision based on repeat analyses of secondary  
491 standard VG2) in the top-right corner.

492 The more primitive basaltic melt inclusions have elevated volatile concentrations compared to  
493 mid-ocean ridge basalts, reflecting the influence of a subducted slab component added to the  
494 mantle wedge source (Figure 5; e.g., Wysoczanski et al., 2006). The maximum volatile content  
495 of basaltic-andesite melt inclusions is similar (H<sub>2</sub>O, Cl) or greatly exceed (CO<sub>2</sub>, S) volatile  
496 concentrations in OVC rhyolites (Figure 5; e.g., Johnson et al., 2011). This supports the  
497 inference that basalts exchange volatiles with rhyolitic magmas during crustal interactions  
498 (e.g., Leonard et al., 2002; Shane et al., 2008a, 2008b, 2007).

499 For Tarawera and Rotokawau, melt inclusions can be divided into two sub-groups based on S  
500 concentrations above and below ~1000 ppm (Figure 5g), which requires two separate  
501 crystallisation regimes as previously proposed by Rowe et al. (2021). We suggest that these  
502 regimes correspond to isobaric cooling and decompression-induced degassing (Figure 5g).  
503 Concentrations of S and Cl increase in the melt during crystallisation for melt inclusions with  
504 >1000 ppm S (Figure 5g). This behaviour indicates these elements behaved incompatibly (i.e.,  
505 were not partitioned into crystallising minerals or exsolved fluids), such that fluid-melt bulk  
506 partition coefficients for S and Cl at these conditions were very low (e.g., Gennaro et al., 2021;  
507 O'Neill, 2020; Tattitch et al., 2021; Thomas and Wood, 2021). Rotokawau and Tarawera melt  
508 inclusions with <1000 ppm S show increasing Cl with decreasing S (Figure 5g). Decreasing  
509 pressure during ascent drives crystallisation and degassing, forming a fluid that sequesters S,  
510 but not Cl (e.g., Lesne et al., 2011). In summary, the parent basalt is volatile-rich, suggesting

511 derivation from high-degrees of fluid flux melting associated with caldera regions (cf. Barker  
512 et al., 2020, and Zellmer et al., 2020).

513

### 514 5.1.3 Similar storage conditions and volatiles prior to eruptions of varying style

515 Despite the similar pre-eruptive compositions and conditions of the basaltic magma, there is a  
516 wide variation in eruption style (Figure 1b and Figure 6). Bamber et al. (2019) suggested  
517 moderate storage temperatures (<1100 °C) are important for generating basaltic Plinian  
518 eruptions. These are shown to occur at Tarawera but are also found for the smaller intensity  
519 eruptions (Figure 6). Volatile concentrations (H<sub>2</sub>O, Cl, and S) and trends are also similar between  
520 basaltic eruptions around the OVC (Figure 5). High H<sub>2</sub>O concentrations and H<sub>2</sub>O exsolution  
521 have been suggested to drive basaltic Plinian eruptions (Bamber et al., 2019; Pérez et al., 2020).  
522 However, high H<sub>2</sub>O concentrations are found across the range of eruption styles at Okataina  
523 and are therefore not unique to Tarawera (Figure 5a and f). Both Rotokawau and Tarawera  
524 have a population of melt inclusions that display degassing trends, and this population may  
525 have been missed at Terrace Rd where fewer melt inclusions were analysed (Figure 5g). It has  
526 been suggested that melt inclusions from Plinian eruptions record a unique degassing path  
527 (Moretti et al., 2018) compared to other explosive eruptions. Moretti et al. (2018) suggest lower  
528 Cl but higher S occurs in less explosive eruptions compared to more explosive eruptions due  
529 to the differences in dehydration and sulphide-saturation that occur during crystallisation.  
530 However, the observed differences in S and Cl concentration around the OVC do not relate to  
531 eruption style: Rotokawau has higher S and Cl but eruption intensity intermediate between  
532 Terrace Rd and Tarawera, and there is no evidence for sulphide-saturation (Figure 5g). High  
533 CO<sub>2</sub> concentrations are thought to be important for generating (sub-)Plinian basaltic eruptions  
534 (e.g., Allison et al., 2021; Sable et al., 2009), which could be important around the OVC.  
535 Unfortunately, our CO<sub>2</sub> data for Tarawera are likely compromised by bubble formation and we  
536 do not have sufficient data to compare against smaller eruptions (Figure 5f).

537 External factors could also influence eruption style of basaltic magmas. Basaltic eruptions  
538 around the OVC are thought to be modulated by crustal faults, as evidenced by the linear nature  
539 of their eruptive vents underlain by dikes (Nairn and Cole, 1981). There is also evidence of  
540 volcano-tectonic interactions for OVC rhyolitic eruptions (e.g., Berryman et al., 2022;  
541 Villamor et al., 2022). Hence, these eruptions may be triggered by earthquakes, especially  
542 given the high melt H<sub>2</sub>O contents and mushy-nature of storage (e.g., Hamling and Kilgour,  
543 2020; Seropian et al., 2021). Additionally, the presence and physical state (e.g., viscosity) of  
544 large silicic bodies in the crust could affect basaltic eruption style by impeding (or not) the  
545 ascent of basaltic magmas to the surface. Tectonics in addition to the complex nature of the  
546 crust around the OVC may therefore be important for generating the wide variety of basaltic  
547 eruption styles observed.

548

### 549 5.1.4 Mixing and entrainment during ascent influenced by eruption style

550 Samples analysed in this study clearly point to variable extents of basaltic magma mixing prior  
551 to eruption (and also entrainment of xenocrystic high-An plagioclase described in Section 5.2).  
552 The implication is that a magma interacted with multiple different gabbroic bodies as it  
553 ascended through the crust, entraining crystals *en route*. This is also seen in differences in  
554 oxygen isotope compositions between crystals and groundmass in these eruptions (Law et al.,  
555 *in review*). The timescales of interactions were likely very short (e.g., to preserve multiple  
556 groundmass textures and produce the sharp rims of lower-An plagioclase around high-An  
557 plagioclase, Figure 2c and e–h), and probably occurred during pre-eruptive magma ascent. The  
558 proportion of crystals entrained is likely correlated with magma ascent rate, which potentially

559 controls eruption style. Lower intensity eruptions (Terrace Road, Rotokawau) contain a high  
560 proportion of macrocrysts, whereas Tarawera has a negligible crystal cargo (0.5 vol%, Sable  
561 et al., 2009). The melt entrained more crystals as it passed through the mush layers in smaller  
562 eruptions than in the Plinian eruption. This difference likely reflects the faster ascent rate of  
563 Plinian magmas, rather than the cause *per se* of varying eruption style.

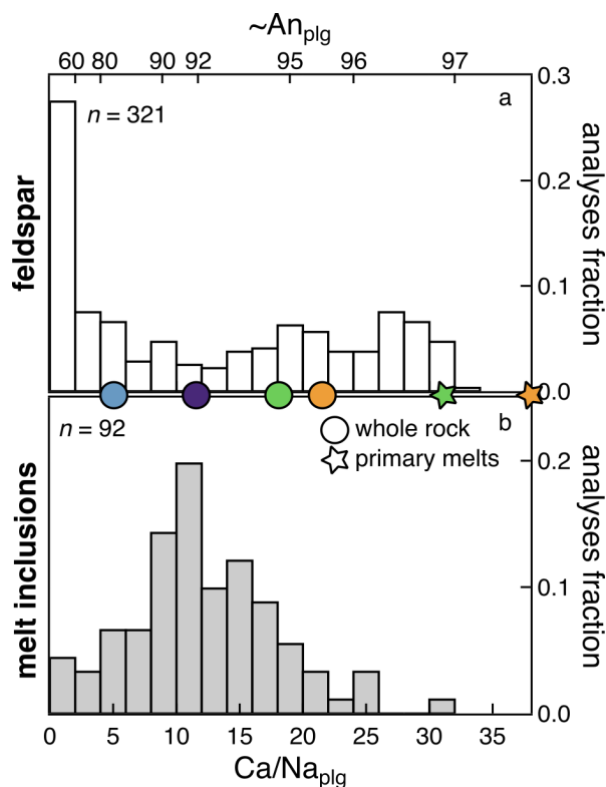
564 OVC basalts eruptions additionally show entrainment of rhyolitic material (e.g., low-Mg#  
565 orthopyroxene, low-An plagioclase, quartz, alkali feldspars, and rhyolitic melt inclusions),  
566 similar in composition to OVC rhyolitic eruptions (Figure 3 and Figure 4). Rhyolitic material  
567 appear to have been incorporated at a late-stage of magma ascent (e.g., sharp boundaries  
568 between basaltic and rhyolitic material, Figure 2p), probably when the basaltic magma ascended  
569 and briefly mingled with previously erupted, and relatively cold rhyolite domes (i.e., solid  
570 material in the crust or erupted at the surface, then buried).

571 The diversity of magma types and mixing dynamics evident in individual eruptions and across  
572 eruptions reflects the interplay between basaltic magma ascent rates and the distribution,  
573 composition, and rheological state of magma bodies both vertically and horizontally. As  
574 mixing timescales appear to be short, precursory signals to basaltic explosive eruptions could  
575 be limited, as recorded by the very short precursory signals observed in the days before the  
576 Tarawera 1886 C.E. eruption (Keam, 1988).

577

## 578 5.2 High-An plagioclase xenocrysts

579 High-An (>An<sub>90</sub>) plagioclase grains are found in all OVC eruptions and basaltic material since  
580 ~55 ka, but also in basaltic material from the ~26.5 ka TVC Oruanui eruption (Allan et al.,  
581 2017; Rooyackers et al., 2018; Wilson et al., 2006) and the ~330 ka OVC post-caldera deposits  
582 following the Matahina eruption (Deering et al., 2011). Therefore, these high-An plagioclase  
583 grains are preserved in spatially and temporally separated OVC (and TVC) basalts. To explain  
584 this ubiquity, these high-An plagioclase crystals must be derived from a common source or  
585 conditions. Thin, low-An rims surrounding high-An plagioclase indicates disequilibrium  
586 (Figure 2e–h), suggesting the high-An plagioclase are xenocrysts (Figure 3k–o). Additionally,  
587 <sup>87</sup>Sr/<sup>86</sup>Sr ratios for high-An plagioclases are distinctly more radiogenic than the groundmass,  
588 affirming that they are derived from a separate source (Rowe et al., 2021). High-An plagioclase  
589 (>An<sub>96</sub>) crystals are likely to have crystallised from most primitive TVZ basalts (Wilson et al.,  
590 2006; Zellmer et al. (2020), rather than melt inclusions or average whole rock compositions for  
591 each eruption (Figure 8; calculation details are given in Supplementary Material using Sisson  
592 and Grove, 1993).



593

594 *Figure 8* Ca/Na ratios in plagioclase (and approximate An): (a) from all analysed grains; and (b) calculated for  
 595 equilibrium with melt inclusions from this study. Symbols are calculated Ca/Na<sub>plg</sub> in equilibrium with average  
 596 whole rock data for each eruption (circles) or primary melt compositions (stars) calculated by Zellmer et al. (2020),  
 597 where symbol colour indicates eruption (Terrace Rd = purple, Rotomakariri = blue, Rotokawau = green, and  
 598 Tarawera = orange). Equilibrium plagioclase compositions from melt compositions are calculated using Sisson  
 599 and Grove (1993) (details in Supplementary Material)

600 High-An plagioclase can be indicative of hydrous conditions or crystallisation from Na-poor  
 601 melts (e.g., Panjasawatwong et al., 1995; Takagi et al., 2005). High magmatic water contents  
 602 would occur as melting is driven by fluid-fluxing of a fertile mantle in active calderas (e.g.,  
 603 Barker et al., 2020; Zellmer et al., 2020). Alternatively, the high-An content could be due to  
 604 high Ca/Na in the melt and not reflect high water contents in the melt (e.g., Panjasawatwong  
 605 et al., 1995); however, there is no evidence for melt with very high Ca/Na in the OVC.  
 606 Inclusions of high-An plagioclase in clinopyroxene indicates plagioclase crystallisation before  
 607 clinopyroxene, which occurs at lower H<sub>2</sub>O. This may reflect the decompression melting source  
 608 that is thought to dominate in intracaldera regions (Barker et al., 2020; Zellmer et al., 2020).  
 609 Hence, decompression melting could also be a minor component of active calderas. However,  
 610 further investigation is needed to distinguish between these different potential sources, in  
 611 particular measuring melt inclusion compositions from these high-An plagioclase grains for  
 612 volatiles and trace elements.

613

### 614 5.3 Rotomakariri

615 Rotomakariri consists of mostly andesite melt inclusions and matrix glass, clinopyroxene, and  
 616 high-Mg# orthopyroxene, but also olivine and both medium- and high-An plagioclase (Figure 3  
 617 and Figure 4). The high-An plagioclase are xenocrystic, as described in Section 5.2.  
 618 Clinopyroxene-melt thermobarometry suggests crystallisation at 1050 ± 18 °C and 5 ± 3 kbar;  
 619 two-pyroxene thermobarometry suggests higher pressures (~6 ± 4 kbar, with large model  
 620 uncertainties of ±3.2 kbar) and overlapping temperatures (~950–1100 °C) (Figure 6). This is  
 621 unusually hot for an andesite. Rhyolite-MELTS modelling indicates that the andesitic melt

622 inclusions and matrix glass can form from a similar initial magma composition as the basalt  
623 characteristic of Tarawera, Terrace Rd, and Rotokawau. However, fractional crystallisation is  
624 to a lower  $T$  (~950 °C), shallower (1 kbar, well below two-pyroxene pressure estimates but  
625 within error of the clinopyroxene-melt barometry), and under more reducing conditions  
626 ( $\Delta\text{NNO}-1$  to 0) (Figure 4d–f).

627 Rotomakariri melt inclusion  $\text{H}_2\text{O}$  contents are very low, but this could indicate diffusive loss  
628 of  $\text{H}_2\text{O}$ , which is supported by many Rotomakariri melt inclusions being crystallised (these  
629 were not analysed; Figure 5a). The low Cl and S concentrations indicate partitioning into a  
630 coexisting fluid (Figure 5b, c, and g). This is expected at low pressures and the hot, dry melt  
631 conditions observed; especially for S in more evolved melt compositions (e.g., Clemente et al.,  
632 2004; Gennaro et al., 2021; O’Neill, 2020; Tattitch et al., 2021; Thomas and Wood, 2021).  
633 Overall, this suggests Rotomakariri was a basaltic magma like Tarawera, Terrace Rd, and  
634 Rotokawau, which had entrained xenocrystic high-An plagioclase. It then stalled at shallow  
635 levels, resulting in low volatile contents and further cooling, crystallising to an andesite melt  
636 composition prior to eruption.

637

## 638 **6 The magmatic architecture around the OVC**

639 The mineral and melt inclusion compositions measured in Tarawera, Terrace Rd, Rotokawau  
640 and Rotomakariri are common to many different OVC eruptions. For instance, similar melt  
641 inclusions (albeit more primitive) and mineral chemistries are found in other basalts from  
642 around the OVC (e.g., Kaharoa, Okareka, Matahi, and Matahina) and even in TVC basaltic  
643 material (e.g., Oraunui), showing that these are common features within the TVZ (Allan et al.,  
644 2017; Barker et al., 2020; Deering et al., 2011; Rooyakkers et al., 2018; Wilson et al., 2006).  
645 As the same basaltic magmas are occurring in eruptions separated spatially and temporally,  
646 these sets of conditions must be common around the OVC even though magmas themselves  
647 were not sourced from the same spatio-temporal reservoirs.

648 Combining the evidence from barometry and mixing textures suggests a crust full of individual  
649 magma reservoirs around the OVC, that are variously sampled during eruption. Despite large  
650 model uncertainties, pressures derived from clinopyroxene-melt and  $\text{H}_2\text{O}-\text{CO}_2$  barometry and  
651 rhyolite-MELTS modelling lie within the TVZ crust assuming a crustal density of  $2700 \text{ kg}\cdot\text{m}^{-3}$   
652 and a Moho at 25–30 km or 7–8 kbar pressure (Bannister et al., 2004). This suggests that  
653 basaltic magmas, in addition to rhyolitic magmas, are stored and evolve polybarically within  
654 the crust. This agrees with current geochemical and geophysical constraints from previous  
655 Tarawera clinopyroxene barometry (1–3 kbar, with some >7 kbar, reported in Sable et al.,  
656 2009) and the presence of partial melt bodies at similar depths around the OVC, such as at 6–  
657 16 km using receiver functions (Bannister et al., 2004), 10–20 km (as shallow as 8 km beneath  
658 Waimungu) using electrical resistivity inversions (Heise et al., 2016, 2010), 8–10 km from  
659 earthquake swarms attributed to a basaltic dike intrusion (Benson et al., 2021), 5–8 km from  
660 lower P-wave velocities (Bannister et al., 2022), and 8–15 km for a complex of relatively mafic  
661 magma from magnetotelluric models (Bertrand et al., 2022). Additionally, conceptual models  
662 based on petrological modelling invoke mafic sheets residing at 11–15 km, with some isolated  
663 pods found at 8–6 km depths (Cole et al., 2014; Deering et al., 2010). Large uncertainties in  
664 clinopyroxene-melt barometry mean individual magma reservoirs cannot be identified using  
665 this method. However, the mineral textures and compositions suggest evolution in isolated  
666 reservoirs, where each batch has its own distinct composition reflecting their individual  
667 histories.

668 These observations suggest that a thick, crustal mush – containing a wealth of individual,  
669 isolated pockets of magmas – is mostly trapping the ascending basalts in the crust that fuel

670 magmatism around the OVC. This model likely applies more generally to active calderas in  
671 the TVZ and is similar to other arc settings, such as the Andean Puna plateau, resulting in the  
672 dominance of compositionally-evolved volcanism (e.g., Delph et al., 2017; Kay et al., 2010).  
673 However, the extensional regime of the TVZ is clearly important in allowing some of these  
674 basalts to reach the surface and erupt explosively.

675 The few basalts that do make it to the surface have passed through the complicated crustal  
676 mush and carry the signature of these interactions in their crystal cargo. This highlights the use  
677 of basaltic mineral and melt inclusion chemistry as windows into the sub-surface in silicic  
678 magmatic regions, extending its application from using olivine-hosted melt inclusions to  
679 understand mantle melting dynamics (e.g., Barker et al., 2020) to analysing clinopyroxene-  
680 hosted melt inclusions to gain insight into crustal processes. Combining data from multiple  
681 eruptions separated spatially and temporally has highlighted that similar processes are  
682 important around the OVC for potentially the last ~30 ka.

683

## 684 **7 Author Contributions**

685 ECH, JDB, HMM, and GK conceived the project idea. ECH and SL collected and processed  
686 the data. All authors contributed to data interpretation. ECH led manuscript production with  
687 further contribution from all authors.

688

## 689 **8 Acknowledgements**

690 We would like to thank the Ruawahia 2B trust for welcoming us onto Mount Tarawera and  
691 permitting us to collect samples on the mountain and especially Ken Raureti, Tīpene Marr, and  
692 Paul Warbrick for their support of this work; Kaingaroa Timberlands for permits to access  
693 Kaingaroa Forest and Waimangu Forest to collect samples; Yves Feisel (now at the University  
694 of Mainz, Germany), Marco Michelini (now at the University of Pittsburgh, USA), Brad Scott  
695 (Te Pū Ao | GNS Science, Aotearoa New Zealand), and Nick Macdonald (Te Pū Ao | GNS  
696 Science, Aotearoa New Zealand) for helping with sample collection; Richard Hinton for his  
697 assistance at the NERC ion microprobe facility at the University of Edinburgh, UK  
698 (IMF560/0515); Stuart Kearns and Ben Buse for their assistance with the electron probe and  
699 SEM at the University of Bristol, UK; three anonymous reviewers for their constructive  
700 reviews that improved the clarity and interpretation of the paper; and Prof. Mike Rowe  
701 (University of Auckland, Aotearoa New Zealand) for their editorial handling of the paper. ECH  
702 was supported by a NERC GW4+ DTP studentship (NE/L002434/1) and is thankful for the  
703 support and additional funding from CASE partner Te Pū Ao | GNS Science, Aotearoa New  
704 Zealand, and a Geology Option Post-Doctoral Fellowship from Caltech, CA USA. SL was  
705 supported by a NERC E<sup>3</sup> DTP studentship (NE/L002558/1). GK and ECH are supported by  
706 the Hazards and Risk Management Programme, which is part of New Zealand Strategic  
707 Science Investment Funding (SSIF) from the New Zealand Ministry of Business, Innovation  
708 & Employment (MBIE). JDB acknowledges support through a Royal Society Research  
709 Professorship.

710

## 711 **9 References**

- 712 Allan, A.S.R., Barker, S.J., Millet, M.A., Morgan, D.J., Rooyackers, S.M., Schipper, C.I., Wilson, C.J.N., 2017.  
713 A cascade of magmatic events during the assembly and eruption of a super-sized magma body. *Contrib. to*  
714 *Mineral. Petrol.* 172, 49. <https://doi.org/10.1007/s00410-017-1367-8>  
715 Allison, C.M., Roggensack, K., Clarke, A.B., 2021. Highly explosive basaltic eruptions driven by CO<sub>2</sub>

716 exsolution. *Nat. Commun.* 12, 217. <https://doi.org/10.1038/s41467-020-20354-2>

717 Annen, C., Blundy, J.D., Sparks, R.S.J., 2006. The Genesis of Intermediate and Silicic Magmas in Deep Crustal  
718 Hot Zones. *J. Petrol.* 47, 505–539. <https://doi.org/10.1093/petrology/egi084>

719 Bamber, E.C., Arzilli, F., Polacci, M., Hartley, M.E., Fellowes, J., Di Genova, D., Chavarría, D., Saballos, J.A.,  
720 Burton, M.R., 2019. Pre- and syn-eruptive conditions of a basaltic Plinian eruption at Masaya Volcano,  
721 Nicaragua: The Masaya Triple Layer (2.1 ka). *J. Volcanol. Geotherm. Res.* 106761.  
722 <https://doi.org/10.1016/J.JVOLGEORES.2019.106761>

723 Bannister, S., Bertrand, E.A., Heimann, S., Bourguignon, S., Asher, C., Shanks, J., Harvison, A., 2022. Imaging  
724 sub-caldera structure with local seismicity, Okataina Volcanic Centre, Taupo Volcanic Zone, using  
725 double-difference seismic tomography. *J. Volcanol. Geotherm. Res.* 431, 107653.  
726 <https://doi.org/10.1016/J.JVOLGEORES.2022.107653>

727 Bannister, S.C., Bryan, C.J., Bibby, H.M., 2004. Shear wave velocity variation across the Taupo Volcanic Zone,  
728 New Zealand, from receiver function inversion. *Geophys. J. Int.* 159, 291–310.  
729 <https://doi.org/10.1111/j.1365-246X.2004.02384.x>

730 Barker, S.J., Rowe, M.C., Wilson, C.J.N., Gamble, J.A., Rooyackers, S.M., Wysoczanski, R.J., Illsley-Kemp,  
731 F., Kenworthy, C.C., 2020. What lies beneath? Reconstructing the primitive magmas fueling voluminous  
732 silicic volcanism using olivine-hosted melt inclusions. *Geology* 48, 504–508.  
733 <https://doi.org/10.1130/G47422.1>

734 Barth, A., Newcombe, M., Plank, T., Gonnermann, H., Hajimirza, S., Soto, G.J., Saballos, A., Hauri, E., 2019.  
735 Magma decompression rate correlates with explosivity at basaltic volcanoes — Constraints from water  
736 diffusion in olivine. *J. Volcanol. Geotherm. Res.* 387, 106664.  
737 <https://doi.org/10.1016/j.jvolgeores.2019.106664>

738 Barth, A., Plank, T., 2021. The Ins and Outs of Water in Olivine-Hosted Melt Inclusions: Hygrometer vs.  
739 Speedometer. *Front. Earth Sci.* 9, 343. <https://doi.org/10.3389/feart.2021.614004>

740 Beanland, S., 1989. The Rotokawau Basalt. University of Otago.

741 Beanland, S., Houghton, B.F., 1978. Rotokawau Tephra : basaltic maars in Okataina Volcanic Centre, Taupo  
742 volcanic zone. *New Zeal. Geol. Surv. Bull.* 37–43.

743 Benson, T.W., Illsley-Kemp, F., Elms, H.C., Hamling, I.J., Savage, M.K., Wilson, C.J.N., Mestel, E.R.H.,  
744 Barker, S.J., 2021. Earthquake Analysis Suggests Dyke Intrusion in 2019 Near Tarawera Volcano, New  
745 Zealand. *Front. Earth Sci.* 8, 604. <https://doi.org/10.3389/feart.2020.606992>

746 Berryman, K., Villamor, P., Nairn, I., Begg, J., Alloway, B. V., Rowland, J., Lee, J., Capote, R., 2022. Volcano-  
747 tectonic interactions at the southern margin of the Okataina Volcanic Centre, Taupō Volcanic Zone, New  
748 Zealand. *J. Volcanol. Geotherm. Res.* 427, 107552. <https://doi.org/10.1016/J.JVOLGEORES.2022.107552>

749 Bertrand, E.A., Kannberg, P., Caldwell, T.G., Heise, W., Constable, S., Scott, B., Bannister, S., Kilgour, G.,  
750 Bennie, S.L., Hart, R., Palmer, N., 2022. Inferring the magmatic roots of volcano-geothermal systems in  
751 the Rotorua Caldera and Okataina Volcanic Centre from magnetotelluric models. *J. Volcanol. Geotherm.*  
752 *Res.* 431, 107645. <https://doi.org/10.1016/J.JVOLGEORES.2022.107645>

753 Blatter, D.L., Sisson, T.W., Hankins, W. Ben, 2013. Crystallization of oxidized, moderately hydrous arc basalt  
754 at mid- to lower-crustal pressures: implications for andesite genesis. *Contrib. to Mineral. Petrol.* 166, 861–  
755 886. <https://doi.org/10.1007/s00410-013-0920-3>

756 Bowyer, D.A., 2001. Petrologic, Geochemical and Isotopic Evolution of Rhyolite Lavas from the Okataina,  
757 Rotorua and Kapenga Volcanic Centres, Taupo Volcanic Zone, New Zealand. University of Waikato.

758 Bucholz, C.E., Gaetani, G.A., Behn, M.D., Shimizu, N., 2013. Post-entrapment modification of volatiles and  
759 oxygen fugacity in olivine-hosted melt inclusions. *Earth Planet. Sci. Lett.* 374, 145–155.  
760 <https://doi.org/10.1016/j.epsl.2013.05.033>

761 Buck, C.E., Higham, T.F.G., Lowe, D.J., 2003. Bayesian tools for tephrochronology:  
762 <http://dx.doi.org/10.1191/0959683603hl652ft> 13, 639–647. <https://doi.org/10.1191/0959683603HL652FT>

763 Burt, R.M., Brown, S.J.A., Cole, J.W., Shelley, D., Waight, T.E., 1998. Glass-bearing plutonic fragments from  
764 ignimbrites of the Okataina caldera complex, Taupo Volcanic Zone, New Zealand: remnants of a partially  
765 molten intrusion associated with preceding eruptions. *J. Volcanol. Geotherm. Res.* 84, 209–237.  
766 [https://doi.org/10.1016/S0377-0273\(98\)00039-0](https://doi.org/10.1016/S0377-0273(98)00039-0)

767 Carey, R.J., Houghton, B.F., Sable, J.E., Wilson, C.J.N., 2007. Contrasting grain size and componentry in  
768 complex proximal deposits of the 1886 Tarawera basaltic Plinian eruption. *Bull. Volcanol.* 69, 903–926.  
769 <https://doi.org/10.1007/s00445-007-0117-6>

770 Clemente, B., SCAILLET, B., PICHAVANT, M., 2004. The Solubility of Sulphur in Hydrous Rhyolitic Melts.  
771 *J. Petrol.* 45, 2171–2196. <https://doi.org/10.1093/petrology/egh052>

772 Cole, J.W., 1979. Structure, petrology, and genesis of Cenozoic volcanism, Taupo Volcanic Zone, New  
773 Zealand—a review. *New Zeal. J. Geol. Geophys.* 22, 631–657.  
774 <https://doi.org/10.1080/00288306.1979.10424173>

775 Cole, J.W., 1973a. High-alumina basalts of Taupo Volcanic Zone, New Zealand. *Lithos* 6, 53–64.

776 [https://doi.org/10.1016/0024-4937\(73\)90079-0](https://doi.org/10.1016/0024-4937(73)90079-0)

777 Cole, J.W., 1973b. High-alumina basalts of Taupo Volcanic Zone, New Zealand. *LITHOS* 6, 53–64.

778 [https://doi.org/10.1016/0024-4937\(73\)90079-0](https://doi.org/10.1016/0024-4937(73)90079-0)

779 Cole, J.W., 1970a. Structure and eruptive history of the Tarawera Volcanic Complex. *New Zeal. J. Geol. Geophys.* 13, 879–902. <https://doi.org/10.1080/00288306.1970.10418208>

780

781 Cole, J.W., 1970b. Petrology of the basic rocks of the Tarawera Volcanic Complex. *New Zeal. J. Geol. Geophys.* 13, 925–936. <https://doi.org/10.1080/00288306.1970.10418210>

782

783 Cole, J.W., Deering, C.D., Burt, R.M., Sewell, S., Shane, P.A., Matthews, N.E., 2014. Okataina Volcanic Centre, Taupo Volcanic Zone, New Zealand: A review of volcanism and synchronous pluton development in an active, dominantly silicic caldera system. *Earth-Science Rev.* 128, 1–17.

784

785 <https://doi.org/10.1016/j.earscirev.2013.10.008>

786

787 Collins, N., Rowe, M.C., Kilgour, G., Nichols, A.R.L., Schipper, C.I., Tari, D., Garaebiti, E., 2022. A Petrologic Insight into Transitioning Eruption Styles from the Devil’s Rock Region, Ambae, Vanuatu. *J. Petrol.* 63, 1–22. <https://doi.org/10.1093/PETROLOGY/EGAC050>

788

789 Danyushevsky, L., Della-Pasqua, F.N., Sokolov, S., 2000. Re-equilibration of melt inclusions trapped by magnesian olivine phenocrysts from subduction-related magmas: Petrological implications. *Contrib. to Mineral. Petrol.* 138, 68–83. <https://doi.org/10.1007/PL00007664>

790

791 Danyushevsky, L., Sobolev, A.V., Dmitriev, L.V., 1988. Orthopyroxene-bearing low-Ti tholeiites: The new type of ceanic ridge tholeiite. *Trans. USSR Acad. Sci. Earth Sci. Sect.* 292, 102–105.

792

793 Darragh, M.B., Cole, J.W., Nairn, I.A., Shane, P.A., 2006. Pyroclastic stratigraphy and eruption dynamics of the 21.9 ka Okareka and 17.6 ka Rerewhakaaitu eruption episodes from Tarawera Volcano, Okataina Volcanic Centre, New Zealand. *New Zeal. J. Geol. Geophys.* 49, 309–328.

794

795 <https://doi.org/10.1080/00288306.2006.9515170>

796

797 Davis, W.J., 1985. Geochemistry and petrology of the Rotoiti and Earthquake Flat pyroclastic deposits. University of Auckland.

798

799

800 Deering, C.D., Cole, J.W., Vogel, T.A., 2011. Extraction of crystal-poor rhyolite from a hornblende-bearing intermediate mush: A case study of the caldera-forming Matahina eruption, Okataina volcanic complex. *Contrib. to Mineral. Petrol.* 161, 129–151. <https://doi.org/10.1007/s00410-010-0524-0>

801

802 Deering, C.D., Gravley, D.M., Vogel, T.A., Cole, J.W., Leonard, G.S., 2010. Origins of cold-wet-oxidizing to hot-dry-reducing rhyolite magma cycles and distribution in the Taupo Volcanic Zone, New Zealand. *Contrib. to Mineral. Petrol.* 160, 609–629. <https://doi.org/10.1007/s00410-010-0496-0>

803

804 Delph, J.R., Ward, K.M., Zandt, G., Ducea, M.N., Beck, S.L., 2017. Imaging a magma plumbing system from MASH zone to magma reservoir. *Earth Planet. Sci. Lett.* 457, 313–324.

805

806 <https://doi.org/10.1016/J.EPSL.2016.10.008>

807

808 Ducea, M.N., Saleeby, J.B., Bergantz, G., 2015. The Architecture, Chemistry, and Evolution of Continental Magmatic Arcs. <http://dx.doi.org/10.1146/annurev-earth-060614-105049> 43, 299–331.

809

810 <https://doi.org/10.1146/ANNUREV-EARTH-060614-105049>

811

812 Dungan, M.A., Rhodes, J.M., 1978. Residual glasses and melt inclusions in basalts from DSDP Legs 45 and 46: Evidence for magma mixing. *Contrib. to Mineral. Petrol.* 67, 417–431.

813

814 <https://doi.org/10.1007/BF00383301>

815

816 Foden, J.D., Green, D.H., 1992. Possible role of amphibole in the origin of andesite: some experimental and natural evidence. *Contrib. to Mineral. Petrol.* 109, 479–493. <https://doi.org/10.1007/BF00306551>

817

818 Froggatt, P.C., Lowe, D.J., 1990. A review of late Quaternary silicic and some other tephra formations from New Zealand: Their stratigraphy, nomenclature, distribution, volume, and age. *New Zeal. J. Geol. Geophys.* 33, 89–109. <https://doi.org/10.1080/00288306.1990.10427576>

819

820 Gaetani, G.A., O’Leary, J.A., Shimizu, N., Bucholz, C.E., Newville, M., 2012. Rapid reequilibration of H<sub>2</sub>O and oxygen fugacity in olivine-hosted melt inclusions. *Geology* 40, 915–918.

821

822 <https://doi.org/10.1130/G32992.1>

823

824 Gaetani, G.A., Watson, E.B., 2002. Modeling the major-element evolution of olivine-hosted melt inclusions. *Chem. Geol.* 183, 25–41. [https://doi.org/10.1016/S0009-2541\(01\)00370-9](https://doi.org/10.1016/S0009-2541(01)00370-9)

825

826 Gaetani, G.A., Watson, E.B., 2000. Open system behavior of olivine-hosted melt inclusions. *Earth Planet. Sci. Lett.* 183, 27–41. [https://doi.org/10.1016/S0012-821X\(00\)00260-0](https://doi.org/10.1016/S0012-821X(00)00260-0)

827

828 Gamble, J.A., Smith, I.E.M., Graham, I.J., Peter Kokelaar, B., Cole, J.W., Houghton, B.F., Wilson, C.J.N., 1990. The petrology, phase relations and tectonic setting of basalts from the taupo volcanic zone, New Zealand and the Kermadec Island arc - havre trough, SW Pacific. *J. Volcanol. Geotherm. Res.* 43, 253–270. [https://doi.org/10.1016/0377-0273\(90\)90055-K](https://doi.org/10.1016/0377-0273(90)90055-K)

829

830

831 Gamble, J.A., Smith, I.E.M., McCulloch, M.T., Graham, I.J., Kokelaar, B.P., 1993. The geochemistry and petrogenesis of basalts from the Taupo Volcanic Zone and Kermadec Island Arc, S.W. Pacific. *J. Volcanol. Geotherm. Res.* 54, 265–290. [https://doi.org/10.1016/0377-0273\(93\)90067-2](https://doi.org/10.1016/0377-0273(93)90067-2)

832

833

834

835 Gennaro, E., Paonita, A., Iacono-Marziano, G., Moussallam, Y., Pichavant, M., Peters, N., Martel, C., 2020.



836 Sulphur Behaviour and Redox Conditions in Etnean Magmas during Magma Differentiation and  
837 Degassing. *J. Petrol.* 61, ega095. <https://doi.org/10.1093/PETROLOGY/EGAA095>

838 Ghiorso, M.S., Gualda, G.A.R., 2015. An H<sub>2</sub>O–CO<sub>2</sub> mixed fluid saturation model compatible with rhyolite-  
839 MELTS. *Contrib. to Mineral. Petrol.* 169, 53. <https://doi.org/10.1007/s00410-015-1141-8>

840 Graham, I.J., Cole, J.W., Briggs, R.M., Gamble, J.A., Smith, I.E.M., 1995. Petrology and petrogenesis of  
841 volcanic rocks from the Taupo Volcanic Zone: a review. *J. Volcanol. Geotherm. Res.* 68, 59–87.  
842 [https://doi.org/10.1016/0377-0273\(95\)00008-I](https://doi.org/10.1016/0377-0273(95)00008-I)

843 Grange, L.I., 1937. The geology of the Rotorua-Taupo Subdivision, Rotorua and Kaimanawa Divisions. *New  
844 Zeal. Geol. Surv. Bull.* 37, 1–138.

845 Grove, T.L., Till, C.B., Krawczynski, M.J., 2012. The Role of H<sub>2</sub>O in Subduction Zone Magmatism.  
846 <http://dx.doi.org/10.1146/annurev-earth-042711-105310> 40, 413–439.  
847 <https://doi.org/10.1146/ANNUREV-EARTH-042711-105310>

848 Gualda, G.A.R., Ghiorso, M.S., Lemons, R. V., Carley, T.L., 2012. Rhyolite-MELTS: a Modified Calibration of  
849 MELTS Optimized for Silica-rich, Fluid-bearing Magmatic Systems. *J. Petrol.* 53, 875–890.  
850 <https://doi.org/10.1093/PETROLOGY/EGR080>

851 Hamling, I.J., Kilgour, G., 2020. Goldilocks conditions required for earthquakes to trigger basaltic eruptions:  
852 Evidence from the 2015 Ambrym eruption. *Sci. Adv.* 6, eaaz5261.  
853 <https://doi.org/10.1126/SCIADV.AAZ5261>

854 Hamling, I.J., Kilgour, G., Hreinsdóttir, S., Bertrand, E., Bannister, S., 2022. Estimating the distribution of melt  
855 beneath the Okataina Caldera, New Zealand: An integrated approach using geodesy, seismology and  
856 magnetotellurics. *J. Volcanol. Geotherm. Res.* 426, 107549.  
857 <https://doi.org/10.1016/J.JVOLGEORES.2022.107549>

858 Hartley, M.E., MacLennan, J., Edmonds, M., Thordarson, T., 2014. Reconstructing the deep CO<sub>2</sub> degassing  
859 behaviour of large basaltic fissure eruptions. *Earth Planet. Sci. Lett.* 393, 120–131.  
860 <https://doi.org/10.1016/j.epsl.2014.02.031>

861 Hartley, M.E., Neave, D.A., MacLennan, J., Edmonds, M., Thordarson, T., 2015. Diffusive over-hydration of  
862 olivine-hosted melt inclusions. *Earth Planet. Sci. Lett.* 425, 168–178.  
863 <https://doi.org/10.1016/J.EPSL.2015.06.008>

864 Heise, W., Caldwell, T.G., Bertrand, E.A., Hill, G.J., Bennie, S.L., Palmer, N.G., 2016. Imaging the deep source  
865 of the Rotorua and Waimangu geothermal fields, Taupo Volcanic Zone, New Zealand. *J. Volcanol.  
866 Geotherm. Res.* 314, 39–48. <https://doi.org/10.1016/j.jvolgeores.2015.10.017>

867 Heise, W., Caldwell, T.G., Bibby, H.M., Bennie, S.L., 2010. Three-dimensional electrical resistivity image of  
868 magma beneath an active continental rift, Taupo Volcanic Zone, New Zealand. *Geophys. Res. Lett.* 37,  
869 n/a-n/a. <https://doi.org/10.1029/2010GL043110>

870 Hiess, J., Cole, J.W., Spinks, K.D., 2007. Influence of the crust and crustal structure on the location and  
871 composition of high-alumina basalts of the Taupo Volcanic Zone, New Zealand. *New Zeal. J. Geol.  
872 Geophys.* 50, 327–342. <https://doi.org/10.1080/00288300709509840>

873 Hogg, A.G., Higham, T.F.G., Lowe, D.J., Palmer, J.G., Reimer, P.J., Newnham, R.M., 2003. A wiggle-match  
874 date for Polynesian settlement of New Zealand. *Antiquity* 77, 116–125.  
875 <https://doi.org/10.1017/S0003598X00061408>

876 Hopkins, J.L., Lowe, D.J., Horrocks, J.L., 2021. Tephrochronology in Aotearoa New Zealand.  
877 <https://doi.org/10.1080/00288306.2021.1908368> 64, 153–200.  
878 <https://doi.org/10.1080/00288306.2021.1908368>

879 Houghton, B.F., Hackett, W.R., 1984. Strombolian and phreatomagmatic deposits of Ohakune craters, Ruapehu,  
880 New Zealand: A complex interaction between external water and rising basaltic magma. *J. Volcanol.  
881 Geotherm. Res.* 21, 207–231. [https://doi.org/10.1016/0377-0273\(84\)90023-4](https://doi.org/10.1016/0377-0273(84)90023-4)

882 Houghton, B.F., Wilson, C.J.N., McWilliams, M.O., Lanphere, M.A., Weaver, S.D., Briggs, R.M., Pringle,  
883 M.S., 1995. Chronology and dynamics of a large silicic magmatic system: central Taupo Volcanic Zone,  
884 New Zealand. *Geology* 23, 13–16. [https://doi.org/10.1130/0091-  
885 7613\(1995\)023<0013:CADOAL>2.3.CO;2](https://doi.org/10.1130/0091-7613(1995)023<0013:CADOAL>2.3.CO;2)

886 Hughes, E.C., Buse, B., Kearns, S.L., Blundy, J.D., Kilgour, G., Mader, H.M., 2019a. Low analytical totals in  
887 EPMA of hydrous silicate glass due to sub-surface charging: Obtaining accurate volatiles by difference.  
888 *Chem. Geol.* 505, 48–56. <https://doi.org/10.1016/J.CHEMGEO.2018.11.015>

889 Hughes, E.C., Mazot, A., Kilgour, G., Asher, C., Michelini, M., Britten, K., Chardot, L., Feisel, Y., Werner, C.,  
890 2019b. Understanding Degassing Pathways Along the 1886 Tarawera (New Zealand) Volcanic Fissure by  
891 Combining Soil and Lake CO<sub>2</sub> Fluxes. *Front. Earth Sci.* 7, 264. <https://doi.org/10.3389/feart.2019.00264>

892 Jackson, M.D., Blundy, J., Sparks, R.S.J., 2018. Chemical differentiation, cold storage and remobilization of  
893 magma in the Earth's crust. *Nature* 564, 405–409. <https://doi.org/10.1038/s41586-018-0746-2>

894 Johnson, E.R., Kamenetsky, V.S., McPhie, J., Wallace, P.J., 2011. Degassing of the H<sub>2</sub>O-rich rhyolites of the  
895 Okataina Volcanic Center, Taupo Volcanic Zone, New Zealand. *Geology* 39, 311–314.

- 896 <https://doi.org/10.1130/G31543.1>
- 897 Kay, S.M., Coira, B.L., Caffè, P.J., Chen, C.H., 2010. Regional chemical diversity, crustal and mantle sources  
898 and evolution of central Andean Puna plateau ignimbrites. *J. Volcanol. Geotherm. Res.* 198, 81–111.  
899 <https://doi.org/10.1016/J.JVOLGEORES.2010.08.013>
- 900 Keam, R.F., 1988. Tarawera: The volcanic eruption of 10 June 1886 A.D. Published by the author, Auckland.
- 901 Kress, V.C., Carmichael, I.S.E., 1991. The compressibility of silicate liquids containing Fe<sub>2</sub>O<sub>3</sub> and the effect of  
902 composition, temperature, oxygen fugacity and pressure on their redox states. *Contrib. to Mineral. Petrol.*  
903 108, 82–92. <https://doi.org/10.1007/BF00307328>
- 904 Laumonier, M., Scaillet, B., Pichavant, M., Champallier, R., Andujar, J., Arbaret, L., 2014. On the conditions of  
905 magma mixing and its bearing on andesite production in the crust. *Nat. Commun.* 2014 5, 1–12.  
906 <https://doi.org/10.1038/ncomms6607>
- 907 Law, S., Bromiley, G.D., Kilgour, G.N., Fitton, J.G., 2021. Tracing mantle source variation through xenocrystic  
908 olivine in the Taupo Volcanic Zone, New Zealand: A role for lithospheric mantle in the shift from  
909 andesitic to rhyolitic compositions. *Lithos* 394–395, 106185.  
910 <https://doi.org/10.1016/J.LITHOS.2021.106185>
- 911 Law, S., Kilgour, G., Bromiley, G.D., Boyce, A.J., n.d. Along arc variation in monogenetic mafic magmas from  
912 the Taupo Volcanic Zone, New Zealand: Insights from the crystal cargo and oxygen isotopes. *J. Petrol.*
- 913 Leonard, G.S., Cole, J.W., Nairn, I.A., Self, S., 2002. Basalt triggering of the c. AD 1305 Kaharoa rhyolite  
914 eruption, Tarawera Volcanic Complex, New Zealand. *J. Volcanol. Geotherm. Res.* 115, 461–486.  
915 [https://doi.org/10.1016/S0377-0273\(01\)00326-2](https://doi.org/10.1016/S0377-0273(01)00326-2)
- 916 Lloyd, A.S., Plank, T., Ruprecht, P., Hauri, E.H., Rose, W., 2013. Volatile loss from melt inclusions in  
917 pyroclasts of differing sizes. *Contrib. to Mineral. Petrol.* 165, 129–153. [https://doi.org/10.1007/s00410-](https://doi.org/10.1007/s00410-012-0800-2)  
918 [012-0800-2](https://doi.org/10.1007/s00410-012-0800-2)
- 919 Lowenstern, J.B., 2003. Melt inclusions come of age: Volatiles, volcanoes, and Sorby’s legacy. *Dev. Volcanol.*  
920 5, 1–21. [https://doi.org/10.1016/S1871-644X\(03\)80021-9](https://doi.org/10.1016/S1871-644X(03)80021-9)
- 921 Lowenstern, J.B., 1995. Applications of silicate-melt inclusions to the study of magmatic volatiles, in:  
922 Thompson, J.F. (Ed.), *Magmas, Fluids and Ore Deposits*. Mineralogical Association of Canada Short  
923 Course Volume No.23. pp. 71–99.
- 924 Maclennan, J., 2017. Bubble formation and decrepitation control the CO<sub>2</sub> content of olivine-hosted melt  
925 inclusions. *Geochemistry, Geophys. Geosystems* 18, 597–616. <https://doi.org/10.1002/2016GC006633>
- 926 Marxer, F., Ulmer, P., Müntener, O., Othmar, 2021. Polybaric fractional crystallisation of arc magmas: an  
927 experimental study simulating trans-crustal magmatic systems. *Contrib. to Mineral. Petrol.* 2021 1771  
928 177, 1–36. <https://doi.org/10.1007/S00410-021-01856-8>
- 929 Mazot, A., Schwandner, F.M., Christenson, B., de Ronde, C.E.J., Inguaggiato, S., Scott, B.J., Graham, D.,  
930 Britten, K., Keeman, J., Tan, K., 2014. CO<sub>2</sub> discharge from the bottom of volcanic Lake Rotomahana,  
931 New Zealand. *Geochemistry, Geophys. Geosystems* 15, 577–588. <https://doi.org/10.1002/2013GC004945>
- 932 Moore, L.R., Gazel, E., Tuohy, R., Lloyd, A.S., Esposito, R., Steele-MacInnis, M., Hauri, E.H., Wallace, P.J.,  
933 Plank, T., Bodnar, R.J., 2015. Bubbles matter: An assessment of the contribution of vapor bubbles to melt  
934 inclusion volatile budgets. *Am. Mineral.* 100, 806–823. <https://doi.org/10.2138/am-2015-5036>
- 935 Moretti, R., Métrich, N., Arienzo, I., Di Renzo, V., Aiuppa, A., Allard, P., 2018. Degassing vs. eruptive styles at  
936 Mt. Etna volcano (Sicily, Italy). Part I: Volatile stocking, gas fluxing, and the shift from low-energy to  
937 highly explosive basaltic eruptions. *Chem. Geol.* 482, 1–17.  
938 <https://doi.org/10.1016/J.CHEMGEO.2017.09.017>
- 939 Mortimer, N., Campbell, H.J., Tulloch, A.J., King, P.R., Stagpoole, V.M., Wood, R.A., Rattenbury, M.S.,  
940 Sutherland, R., Adams, C.J., Collot, J., Seton, M., 2017. Zealandia: Earth’s hidden Continent. *GSA Today*  
941 27, 27–35. <https://doi.org/10.1130/GSATG321A.1>
- 942 Müntener, O., Ulmer, P., 2018. Arc crust formation and differentiation constrained by experimental petrology.  
943 *Am. J. Sci.* 318, 64–89. <https://doi.org/10.2475/01.2018.04>
- 944 Nairn, I.A., 2002. *Geology of the Okataina Volcanic Centre, scale 1:50 000*. Institute of Geological and Nuclear  
945 Sciences Limited.
- 946 Nairn, I.A., 1992. The Te Rere and Okareka eruptive episodes — Okataina Volcanic Centre, Taupo Volcanic  
947 Zone, New Zealand. *New Zeal. J. Geol. Geophys.* 35, 93–108.  
948 <https://doi.org/10.1080/00288306.1992.9514503>
- 949 Nairn, I.A., 1981. *Some Studies of the Geology, Volcanic History, and Geothermal Resources of the Okataina*  
950 *Volcanic Centre, Taupo Volcanic Zone, New Zealand*. Victoria University of Wellington, Wellington.
- 951 Nairn, I.A., 1979. Rotomahana—Waimangu eruption, 1886: base surge and basalt magma. *New Zeal. J. Geol.*  
952 *Geophys.* 22, 363–378. <https://doi.org/10.1080/00288306.1979.10424105>
- 953 Nairn, I.A., Cole, J.W., 1981. Basalt dikes in the 1886 Tarawera Rift. *New Zeal. J. Geol. Geophys.* 24, 585–592.  
954 <https://doi.org/10.1080/00288306.1981.10421534>
- 955 Nairn, I.A., Self, S., Cole, J.W., Leonard, G.S., Scutter, C., 2001. Distribution, stratigraphy, and history of

956 proximal deposits from the c. AD 1305 Kaharoa eruptive episode at Tarawera Volcano, New Zealand.  
957 New Zeal. J. Geol. Geophys. 44, 467–484. <https://doi.org/10.1080/00288306.2001.9514950>

958 Nairn, I.A., Shane, P.A., Cole, J.W., Leonard, G., Self, S., Pearson, N., 2004. Rhyolite magma processes of the  
959 ~AD 1315 Kaharoa eruption episode, Tarawera volcano, New Zealand. J. Volcanol. Geotherm. Res. 131,  
960 265–294. [https://doi.org/10.1016/S0377-0273\(03\)00381-0](https://doi.org/10.1016/S0377-0273(03)00381-0)

961 Nandedkar, R.H., Ulmer, P., Müntener, O., 2014. Fractional crystallization of primitive, hydrous arc magmas:  
962 An experimental study at 0.7 GPa. Contrib. to Mineral. Petrol. 167, 1–27. <https://doi.org/10.1007/s00410-014-1015-5>

964 Neave, D.A., Putirka, K.D., 2017. A new clinopyroxene-liquid barometer, and implications for magma storage  
965 pressures under Icelandic rift zones. Am. Mineral. 102, 777–794. <https://doi.org/10.2138/am-2017-5968>

966 Newnham, R.M., Eden, D.N., Lowe, D.J., Hendy, C.H., 2003. Rerewhakaaitu Tephra, a land–sea marker for the  
967 Last Termination in New Zealand, with implications for global climate change. Quat. Sci. Rev. 22, 289–  
968 308. [https://doi.org/10.1016/S0277-3791\(02\)00137-3](https://doi.org/10.1016/S0277-3791(02)00137-3)

969 Nielsen, R.L., Michael, P.J., Sours-Page, R., 1998. Chemical and physical indicators of compromised melt  
970 inclusions. Geochim. Cosmochim. Acta 62, 831–839. [https://doi.org/10.1016/S0016-7037\(98\)00024-6](https://doi.org/10.1016/S0016-7037(98)00024-6)

971 O’Neill, H.S.C., 2021. The thermodynamic controls on sulfide saturation in silicate melts with application to  
972 Ocean Floor Basalts., in: Moretti, R., Neuville, D.R. (Eds.), Magma Redox Geochemistry, Geophysical  
973 Monograph Series. John Wiley & Sons, Inc., pp. 177–213. <https://doi.org/10.1002/9781119473206.ch10>

974 Panjasawatwong, Y., Danyushevsky, L. V., Crawford, A.J., Harris, K.L., 1995. An experimental study of the  
975 effects of melt composition on plagioclase-melt equilibria at 5 and 10 kbar: implications for the origin of  
976 magmatic high-An plagioclase. Contrib. to Mineral. Petrol. 118, 420–432.  
977 <https://doi.org/10.1007/s004100050024>

978 Pérez, W., Freundt, A., Kutterolf, S., 2020. The basaltic plinian eruption of the ~6 ka San Antonio Tephra and  
979 formation of the Masaya caldera, Nicaragua. J. Volcanol. Geotherm. Res. 401, 106975.  
980 <https://doi.org/10.1016/j.jvolgeores.2020.106975>

981 Peti, L., Hopkins, J.L., Augustinus, P.C., 2021. Revised tephrochronology for key tephtras in the 130-ka Ōrākei  
982 Basin maar core, Auckland Volcanic Field, New Zealand: implications for the timing of climatic changes.  
983 <https://doi.org/10.1080/00288306.2020.1867200> 64, 235–249.  
984 <https://doi.org/10.1080/00288306.2020.1867200>

985 Pittari, A., Muir, S.L., Hendy, C.H., 2016. Lake-floor sediment texture and composition of a hydrothermally-  
986 active, volcanic lake, Lake Rotomahana. J. Volcanol. Geotherm. Res. 314, 169–181.  
987 <https://doi.org/10.1016/j.jvolgeores.2016.02.025>

988 Price, R.C., Gamble, J.A., Smith, I.E.M., Stewart, R.B., Eggins, S., Wright, I.C., 2005. An integrated model for  
989 the temporal evolution of andesites and rhyolites and crustal development in New Zealand’s North Island.  
990 J. Volcanol. Geotherm. Res. 140, 1–24. <https://doi.org/10.1016/j.jvolgeores.2004.07.013>

991 Pullar, W.A., Nairn, I.A., 1972. Matahi Basaltic Tephra member, Rotoiti Breccia Formation. New Zeal. J. Geol.  
992 Geophys. 15, 446–450. <https://doi.org/10.1080/00288306.1972.10422342>

993 Putirka, K.D., 2008. Thermometers and Barometers for Volcanic Systems. Rev. Mineral. Geochemistry 69, 61–  
994 120. <https://doi.org/10.2138/rmg.2008.69.3>

995 Rasmussen, D.J., Plank, T.A., Wallace, P.J., Newcombe, M.E., Lowenstern, J.B., 2020. Vapor-bubble growth in  
996 olivine-hosted melt inclusions. Am. Mineral. 105, 1898–1919. <https://doi.org/10.2138/am-2020-7377>

997 Roedder, E., 1979. Origin and significance of magmatic inclusions. Bull. Mineral. 102, 487–510.

998 Rooney, T.O., Deering, C.D., 2014. Conditions of melt generation beneath the Taupo Volcanic Zone: The  
999 influence of heterogeneous mantle inputs on large-volume silicic systems. Geology 42, 3–6.  
1000 <https://doi.org/10.1130/G34868.1>

1001 Rooyakkers, S.M., Wilson, C.J.N., Schipper, C.I., Barker, S.J., Allan, A.S.R., 2018. Textural and micro-  
1002 analytical insights into mafic–felsic interactions during the Oruanui eruption, Taupo. Contrib. to Mineral.  
1003 Petrol. 173, 35. <https://doi.org/10.1007/s00410-018-1461-6>

1004 Rose-Koga, E.F., Bouvier, A.S., Gaetani, G.A., Wallace, P.J., Allison, C.M., Andrys, J.A., Angeles de la Torre,  
1005 C.A., Barth, A., Bodnar, R.J., Bracco Gartner, A.J.J., Butters, D., Castillejo, A., Chilson-Parks, B.,  
1006 Choudhary, B.R., Cluzel, N., Cole, M., Cottrell, E., Daly, A., Danyushevsky, L. V., DeVitre, C.L.,  
1007 Drignon, M.J., France, L., Gaborieau, M., Garcia, M.O., Gatti, E., Genske, F.S., Hartley, M.E., Hughes,  
1008 E.C., Iveson, A.A., Johnson, E.R., Jones, M., Kagoshima, T., Katzir, Y., Kawaguchi, M., Kawamoto, T.,  
1009 Kelley, K.A., Koornneef, J.M., Kurz, M.D., Laubier, M., Layne, G.D., Lerner, A., Lin, K.Y., Liu, P.P.,  
1010 Lorenzo-Merino, A., Luciani, N., Magalhães, N., Marschall, H.R., Michael, P.J., Monteleone, B.D.,  
1011 Moore, L.R., Moussallam, Y., Muth, M., Myers, M.L., Narváez, D.F., Navon, O., Newcombe, M.E.,  
1012 Nichols, A.R.L., Nielsen, R.L., Pamukcu, A., Plank, T., Rasmussen, D.J., Roberge, J., Schiavi, F.,  
1013 Schwartz, D., Shimizu, K., Shimizu, N., Thomas, J.B., Thompson, G.T., Tucker, J.M., Ustunisik, G.,  
1014 Waelkens, C., Zhang, Y., Zhou, T., 2021. Silicate melt inclusions in the new millennium: A review of  
1015 recommended practices for preparation, analysis, and data presentation. Chem. Geol. 570, 120145.

1016 <https://doi.org/10.1016/j.chemgeo.2021.120145>

1017 Rowe, M.C., Carey, R.J., White, J.D.L., Kilgour, G., Hughes, E., Ellis, B., Rosseel, J.-B., Segovia, A., 2021.

1018 Tarawera 1886: an integrated review of volcanological and geochemical characteristics of a complex

1019 basaltic eruption. *New Zeal. J. Geol. Geophys.* 64, 296–319.

1020 <https://doi.org/10.1080/00288306.2021.1914118>

1021 Sable, J.E., Houghton, B.F., Wilson, C.J.N., Carey, R.J., 2009. Eruption Mechanisms during the climax of the

1022 Tarawera 1886 basaltic Plinian eruption inferred from microtextural characteristics of the deposits, in:

1023 Thordarson, T., Self, S., Larsen, G., Rowland, S.K., Hoskuldsson, A. (Eds.), *Studies in Volcanology: The*

1024 *Legacy of John Walker*. The Geological Society of London, London, pp. 129–154.

1025 Saper, L.M., Stolper, E.M., 2020. Controlled Cooling-Rate Experiments on Olivine-Hosted Melt Inclusions:

1026 Chemical Diffusion and Quantification of Eruptive Cooling Rates on Hawaii and Mars. *Geochemistry,*

1027 *Geophys. Geosystems* 21. <https://doi.org/10.1029/2019GC008772>

1028 Sas, M., Shane, P., Kuritani, T., Zellmer, G.F., Kent, A.J.R., Nakagawa, M., 2021. Mush, melts and

1029 metasediments: A history of rhyolites from the Okataina Volcanic Centre, New Zealand, as captured in

1030 plagioclase. *J. Petrol.* <https://doi.org/10.1093/ptrology/egab038>

1031 Schiano, P., 2003. Primitive mantle magmas recorded as silicate melt inclusions in igneous minerals. *Earth-*

1032 *Science Rev.* 63, 121–144. [https://doi.org/10.1016/S0012-8252\(03\)00034-5](https://doi.org/10.1016/S0012-8252(03)00034-5)

1033 Schmitz, M.D., Smith, I.E.M., 2004. The Petrology of the Rotoiti Eruption Sequence, Taupo Volcanic Zone: an

1034 Example of Fractionation and Mixing in a Rhyolitic System. *J. Petrol.* 45, 2045–2066.

1035 <https://doi.org/10.1093/ptrology/egh047>

1036 Seropian, G., Kennedy, B.M., Walter, T.R., Ichihara, M., Jolly, A.D., 2021. A review framework of how

1037 earthquakes trigger volcanic eruptions. *Nat. Commun.* 12, 1–13. [https://doi.org/10.1038/s41467-021-](https://doi.org/10.1038/s41467-021-21166-8)

1038 [21166-8](https://doi.org/10.1038/s41467-021-21166-8)

1039 Seward, A., Reeves, R., Alcaraz, S., 2022. Assessment of the surface heat loss from Waimangu Geothermal

1040 Valley: Comparison of terrestrial based assessment techniques with remote sensing. *J. Volcanol.*

1041 *Geotherm. Res.* 430, 107630. <https://doi.org/10.1016/J.JVOLGEORES.2022.107630>

1042 Shane, P.A., Martin, S.B., Smith, V.C., Beggs, K.F., Darragh, M.B., Cole, J.W., Nairn, I.A., 2007. Multiple

1043 rhyolite magmas and basalt injection in the 17.7 ka Rerewhakaaitu eruption episode from Tarawera

1044 volcanic complex, New Zealand. *J. Volcanol. Geotherm. Res.* 164, 1–26.

1045 <https://doi.org/10.1016/j.jvolgeores.2007.04.003>

1046 Shane, P.A., Nairn, I.A., Smith, V.C., 2005. Magma mingling in the ~50 ka Rotoiti eruption from Okataina

1047 Volcanic Centre: implications for geochemical diversity and chronology of large volume rhyolites. *J.*

1048 *Volcanol. Geotherm. Res.* 139, 295–313. <https://doi.org/10.1016/j.jvolgeores.2004.08.012>

1049 Shane, P.A., Nairn, I.A., Smith, V.C., Darragh, M.B., Beggs, K.F., Cole, J.W., 2008a. Silicic recharge of

1050 multiple rhyolite magmas by basaltic intrusion during the 22.6 ka Okareka Eruption Episode, New

1051 Zealand. *Lithos* 103, 527–549. <https://doi.org/10.1016/j.lithos.2007.11.002>

1052 Shane, P.A., Smith, V.C., Nairn, I.A., 2008b. Millennial timescale resolution of rhyolite magma recharge at

1053 Tarawera volcano: insights from quartz chemistry and melt inclusions. *Contrib. to Mineral. Petrol.* 156,

1054 397–411. <https://doi.org/10.1007/s00410-008-0292-2>

1055 Sisson, T.W., Grove, T.L., 1993. Experimental investigations of the role of H<sub>2</sub>O in calc-alkaline differentiation

1056 and subduction zone magmatism. *Contrib. to Mineral. Petrol.* 1993 1132 113, 143–166.

1057 <https://doi.org/10.1007/BF00283225>

1058 Smith, V.C., Shane, P., Nairn, I.A., 2004. Reactivation of a rhyolitic magma body by new rhyolitic intrusion

1059 before the 15.8 ka Rotorua eruptive episode: implications for magma storage in the Okataina Volcanic

1060 Centre, New Zealand. *J. Geol. Soc. London.* 161, 757–772. <https://doi.org/10.1144/0016-764903-092>

1061 Sobolev, A. V., Shimizu, N., 1993. Ultra-depleted primary melt included in an olivine from the Mid-Atlantic

1062 Ridge. *Nature* 363, 151–154. <https://doi.org/10.1038/363151a0>

1063 Sparks, S.R.J., Sigurdsson, H., Wilson, L., 1977. Magma mixing: a mechanism for triggering acid explosive

1064 eruptions. *Nat.* 1977 2675609 267, 315–318. <https://doi.org/10.1038/267315a0>

1065 Storm, S., Shane, P., Schmitt, A.K., Lindsay, J.M., 2011. Contrasting punctuated zircon growth in two syn-

1066 erupted rhyolite magmas from Tarawera volcano: Insights to crystal diversity in magmatic systems. *Earth*

1067 *Planet. Sci. Lett.* 301, 511–520. <https://doi.org/10.1016/J.EPSL.2010.11.034>

1068 Takagi, D., Sato, H., Nakagawa, M., 2005. Experimental study of a low-alkali tholeiite at 1-5 kbar: Optimal

1069 condition for the crystallization of high-An plagioclase in hydrous arc tholeiite. *Contrib. to Mineral.*

1070 *Petrol.* 149, 527–540. <https://doi.org/10.1007/s00410-005-0666-7>

1071 Tattitch, B., Chelle-Michou, C., Blundy, J., Loucks, R.R., 2021. Chemical feedbacks during magma degassing

1072 control chlorine partitioning and metal extraction in volcanic arcs. *Nat. Commun.* 2021 121 12, 1–11.

1073 <https://doi.org/10.1038/s41467-021-21887-w>

1074 Thomas, A.P.W., 1888. Report on the Eruption of Tarawera and Rotomahana, NZ, Government Printer,

1075 Wellington, New Zealand.

1076 Thomas, R.W., Wood, B.J., 2021. The chemical behaviour of chlorine in silicate melts. *Geochim. Cosmochim.*  
1077 *Acta* 294, 28–42. <https://doi.org/10.1016/J.GCA.2020.11.018>

1078 Villamor, B.P., Litchfield, N.J., Gómez-Ortiz, D., Martín-González, F., Alloway, B. V., Berryman, K.R., Clark,  
1079 K.J., Ries, W.F., Howell, A., Ansell, I.A., 2022. Fault ruptures triggered by large rhyolitic eruptions at the  
1080 boundary between tectonic and magmatic rift segments: The Manawahe Fault, Taupō Rift, New Zealand.  
1081 *J. Volcanol. Geotherm. Res.* 427, 107478. <https://doi.org/10.1016/J.JVOLGEORES.2022.107478>

1082 Waight, T.E., Troll, V.R., Gamble, J.A., Price, R.C., Chadwick, J.P., 2017. Hf isotope evidence for variable slab  
1083 input and crustal addition in basalts and andesites of the Taupo Volcanic Zone, New Zealand. *Lithos.*  
1084 <https://doi.org/10.1016/j.lithos.2017.04.009>

1085 Walker, G.P.L., Self, S., Wilson, L., 1984. Tarawera 1886, New Zealand — A basaltic plinian fissure eruption.  
1086 *J. Volcanol. Geotherm. Res.* 21, 61–78. [https://doi.org/10.1016/0377-0273\(84\)90016-7](https://doi.org/10.1016/0377-0273(84)90016-7)

1087 Wallace, P.J., Kamenetsky, V.S., Cervantes, P., 2015. Melt inclusion CO<sub>2</sub> contents, pressures of olivine  
1088 crystallization, and the problem of shrinkage bubbles. *Am. Mineral.* 100, 787–794.  
1089 <https://doi.org/10.2138/am-2015-5029>

1090 Wilson, C.J.N., Blake, S., Charlier, B.L.A., Sutton, A.N., 2006. The 26.5 ka Oruanui Eruption, Taupo Volcano,  
1091 New Zealand: Development, Characteristics and Evacuation of a Large Rhyolitic Magma Body. *J. Petrol.*  
1092 47, 35–69. <https://doi.org/10.1093/petrology/egi066>

1093 Wilson, C.J.N., Gravley, D.M., Leonard, G.S., Rowland, J. V., 2009. Volcanism in the central Taupo Volcanic  
1094 Zone, New Zealand: tempo, styles and controls. *Spec. Publ. IAVCEI* 225–247.  
1095 <https://doi.org/10.1144/IAVCEL002.12>

1096 Wilson, C.J.N., Houghton, B.F., McWilliams, M.O., Lanphere, M.A., Weaver, S.D., Briggs, R.M., 1995.  
1097 Volcanic and structural evolution of Taupo Volcanic Zone, New Zealand: a review. *J. Volcanol.*  
1098 *Geotherm. Res.* 68, 1–28. [https://doi.org/10.1016/0377-0273\(95\)00006-G](https://doi.org/10.1016/0377-0273(95)00006-G)

1099 Wyszczanski, R.J., Wright, I.C., Gamble, J.A., Hauri, E.H., Luhr, J.F., Eggins, S.M., Handler, M.R., 2006.  
1100 Volatile contents of Kermadec Arc–Havre Trough pillow glasses: Fingerprinting slab-derived aqueous  
1101 fluids in the mantle sources of arc and back-arc lavas. *J. Volcanol. Geotherm. Res.* 152, 51–73.  
1102 <https://doi.org/10.1016/J.JVOLGEORES.2005.04.021>

1103 Yang, T.-H.J., Chambefort, I., Mazot, A., Rowe, M., Scott, B., MacDonald, N., Werner, C., Fischer, T., Ronde,  
1104 C. de, n.d. Understanding caldera degassing from a detailed investigation at Lake Rotoiti, Okataina  
1105 Volcanic Centre, New Zealand. *J. Volcanol. Geotherm. Res.*

1106 Zellmer, G.F., Kimura, J.-I., Stirling, C.H., Lube, G., Shane, P.A., Iizuka, Y., 2020. Genesis of recent mafic  
1107 magmatism in the Taupo Volcanic Zone, New Zealand: insights into the birth and death of very large  
1108 volume rhyolitic systems? *J. Petrol.* 61, ega027. <https://doi.org/10.1093/petrology/egaa027>

1109